Original research

Helicobacter pylori promotes colorectal carcinogenesis by deregulating intestinal immunity and inducing a mucus-degrading microbiota signature

Anna Ralser,[1] Alisa Dietl,[1] Sebastian Jarosch,[1,2] Veronika Engelsberger,[1] Andreas Wanisch,[1] Klaus Peter Janssen ,[3] Moritz Middelhoff,[4] Michael Vieth,[5] Michael Quante ,[4,6] Dirk Haller ,[7,8] Dirk H Busch,[1,9] Li Deng,[10,11] Raquel Mejías-Luque ,[1,9] Markus Gerhard [1,9]

► Additional supplemental material is published online only. To view, please visit the journal online (http://dx.doi.org/10.1136/gutjnl-2022-328075).

For numbered affiliations see end of article.

Correspondence to
Professor Markus Gerhard, Institute for Medical Microbiology, Immunology and Hygiene, School of Medicine, Technical University of Munich, München 80333, Germany; markus.gerhard@tum.de

RM-L and MG contributed equally.

Received 15 June 2022
Accepted 19 March 2023
Published Online First 4 April 2023

To cite: Ralser A, Dietl A, Jarosch S, *et al*. *Gut* 2023;**72**:1258–1270.

ABSTRACT

Objective *Helicobacter pylori* infection is the most prevalent bacterial infection worldwide. Besides being the most important risk factor for gastric cancer development, epidemiological data show that infected individuals harbour a nearly twofold increased risk to develop colorectal cancer (CRC). However, a direct causal and functional connection between *H. pylori* infection and colon cancer is lacking.

Design We infected two *Apc*-mutant mouse models and C57BL/6 mice with *H. pylori* and conducted a comprehensive analysis of *H. pylori*-induced changes in intestinal immune responses and epithelial signatures via flow cytometry, chip cytometry, immunohistochemistry and single cell RNA sequencing. Microbial signatures were characterised and evaluated in germ-free mice and via stool transfer experiments.

Results *H. pylori* infection accelerated tumour development in *Apc*-mutant mice. We identified a unique *H. pylori*-driven immune alteration signature characterised by a reduction in regulatory T cells and pro-inflammatory T cells. Furthermore, in the intestinal and colonic epithelium, *H. pylori* induced pro-carcinogenic STAT3 signalling and a loss of goblet cells, changes that have been shown to contribute—in combination with pro-inflammatory and mucus degrading microbial signatures—to tumour development. Similar immune and epithelial alterations were found in human colon biopsies from *H. pylori*-infected patients. Housing of *Apc*-mutant mice under germ-free conditions ameliorated, and early antibiotic eradication of *H. pylori* infection normalised the tumour incidence to the level of uninfected controls.

Conclusions Our studies provide evidence that *H. pylori* infection is a strong causal promoter of colorectal carcinogenesis. Therefore, implementation of *H. pylori* status into preventive measures of CRC should be considered.

WHAT IS ALREADY KNOWN ON THIS TOPIC

⇒ *Helicobacter pylori* infection is the most prevalent bacterial infection worldwide and is the most important risk factor for gastric cancer development.
⇒ Infected individuals harbour a nearly twofold increased risk to develop colorectal cancer (CRC).

WHAT THIS STUDY ADDS

⇒ *H. pylori* infection accelerates intestinal tumour development in *Apc*-mutant mice.
⇒ *H. pylori* infection induces a pro-inflammatory and pro-carcinogenic environment in murine and human colon.
⇒ The observed phenotype was normalised upon eradication therapy and is strongly dependent on microbiota.

HOW THIS STUDY MIGHT AFFECT RESEARCH, PRACTICE OR POLICY

⇒ We provide evidence that *H. pylori* infection is a strong causal promoter of colorectal carcinogenesis and should be included into an adapted risk score for CRC.
⇒ Eradication of *H. pylori* infection might be an effective measure to reduce this risk.

INTRODUCTION

Helicobacter pylori infection affects more than half of the world's population and it is a main risk factor for gastric cancer. *H. pylori* induces a number of alterations in the gastric mucosa that together result in neoplastic transformation of the epithelium. Thus, *H. pylori* infection first triggers a complex plethora of immune cascades, directed towards *H. pylori* and orchestrated by the bacterium itself, which originate from priming at the Peyer's patches and the mesenteric lymph nodes of the small intestine.[1 2] The major pro-inflammatory response towards *H. pylori* consists of a mixed T helper (Th)1 and Th17 response,[1] and is to a large extent related to the presence and activity of a type 4 secretion system,[3] which mediates translocation of the oncogenic and highly immunogenic protein CagA into gastric epithelial cells.[4] This leads to chronic inflammation and results in the activation

of pro-inflammatory signalling pathways such as activating nuclear factor-κB (NF-κB) and signal transducer and activator of transcription 3 (STAT3) signalling, which are major drivers of *H. pylori*-induced gastric carcinogenesis.[5] However, *H. pylori* has evolved counter mechanisms in order to establish and maintain chronic infection, for example, by reprogramming dendritic cells (DCs) to induce regulatory T cells (Treg),[6 7] which counterbalance the local pro-inflammatory response in the stomach,[8] and are involved in protection from allergic asthma.[9] Interestingly, this tolerogenic reprogramming of DCs is partially mediated by CagA, via activation of STAT3.[7] Finally, alterations in gastric microbiota are observed on infection, which seem to contribute to the deleterious events leading to gastric cancer following *H. pylori* infection.[10] This idea is supported by studies using animal models as the insulin-gastrin (INS-GAS) mice, which showed more severe gastric pathology and early development of neoplasia when colonised with *H. pylori* and carrying normal commensal microbiota compared with germ-free INS-GAS mice infected with the bacterium.[11]

Although *H. pylori* infection is limited to the stomach, accumulating epidemiological data indicate an association between *H. pylori* infection and different extragastric diseases.[12] Among those, a higher risk of colorectal cancer (CRC) has been reported to be associated with *H. pylori* infection status.[13] However, the mechanisms that could explain this increased risk have not been elucidated.

In our study, we identify *H. pylori*-specific alterations in gut homeostasis that contribute to colorectal carcinogenesis in mouse models of CRC as well as in human samples, and are reversible on *H. pylori* eradication. These findings provide a basis for assessing *H. pylori* status for gastric, and for colon cancer prevention programmes.

RESULTS

H. pylori promotes intestinal carcinogenesis in *adenomatous polyposis coli* mouse models

To determine whether *H. pylori* infection promotes the development of tumours in the lower gastrointestinal (GI) tract, we infected $Apc^{+/min}$ and $Apc^{+/1638N}$ mice for different time periods (online supplemental figure 1A,B). Unexpectedly, $Apc^{+/min}$ mice were highly susceptible to the infection, with only 60% of the mice surviving after 12 weeks of *H. pylori* infection (figure 1A). An increased tumour burden in the small intestine and colon was observed in infected $Apc^{+/min}$ mice compared with uninfected controls (figure 1B,C). Similar results were observed in $Apc^{+/1638N}$ mice, which developed twice as many tumours after infection, and showed larger tumours in the small intestine (online supplemental figure 1C). Notably, in $Apc^{+/1638N}$ mice, colonic tumours were exclusively detected in *H. pylori*-infected mice (online supplemental figure 1C). These observations demonstrate that *H. pylori* infection promotes the development of intestinal and colonic tumours in tumour-prone mice, while exclusively infecting the stomachs of these mice (online supplemental figure 1B).

H. pylori infection induces a pro-inflammatory response in the intestine

Manipulation of host's T-cell immune responses characterises *H. pylori* infection and is one of the main mechanisms

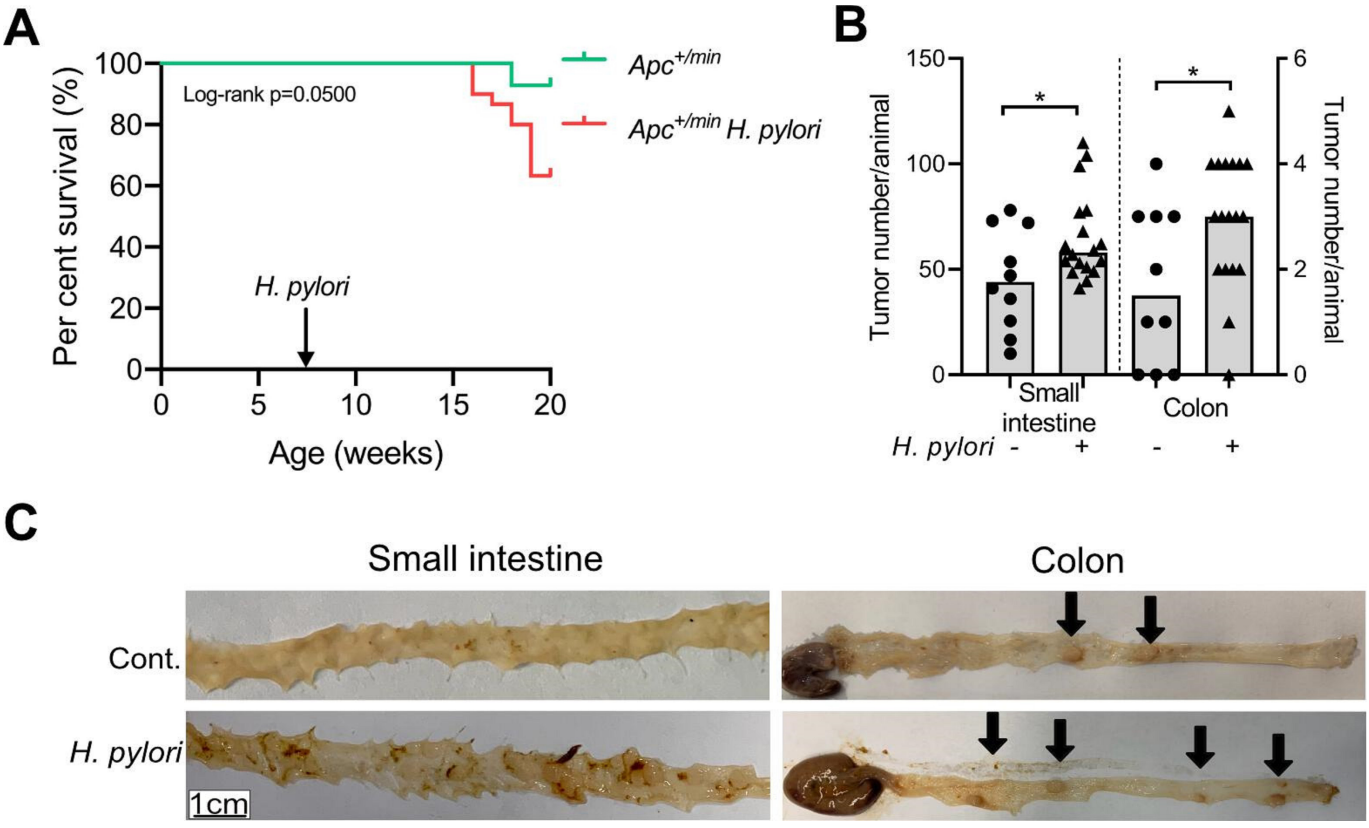

Figure 1 *Helicobacter pylori* promotes intestinal carcinogenesis in *Apc* mouse models. (A) Kaplan-Meier survival curve comparing *H. pylori*-infected and non-infected $Apc^{+/min}$ mice. (B) Tumour counts of *H. pylori*-infected (n=18) and non-infected (n=10) $Apc^{+/min}$ mice in small intestine and colon. (C) Representative pictures of tumours (arrows) in the small intestine and colon of *H. pylori*-infected and non-infected (controls (Cont.)) $Apc^{+/min}$ mice. Each symbol represents one animal, from three independent, pooled experiments. Bars denote median. Statistical significance was determined with Mann-Whitney U test or unpaired t-test, *p<0.05.

contributing to gastric carcinogenesis. To assess whether alterations in intestinal immunity could be related to the increased tumour burden observed in infected *Apc* mutant mice, we first analysed lymphocyte infiltration in the small intestine of $Apc^{+/min}$ and $Apc^{+/1638N}$ mice upon infection (online supplemental figure 1A). Recruitment of intraepithelial $CD3^+$ T cells to small intestine and colon was increased upon *H. pylori* infection (figure 2A and online supplemental figure 2A), wich was also confirmed by flow cytometric analysis of T cells (online supplemental figure 2B,C). Furthermore, this revealed a shift towards more $CD8^+$ and less $CD4^+$ T cells upon infection (online supplemental figure 2D). In addition, the abundance and protein level of $Foxp3^+$ Treg cells was reduced in the small intestine from infected mice compared with uninfected controls, as detected by flow cytometry (figure 2B and online supplemental figure 2E).

To further explore the underlying mechanisms promoting intestinal tumourigenesis upon *H. pylori* infection independently from tumour-prone backgrounds, we infected wild-type C57BL/6 mice (WT) for 24 weeks and analysed immune responses (online supplemental figure 2F). An increased number of intraepithelial $CD3^+$ T cells was also observed in the small intestine as well as in the colon of *H. pylori*-infected WT mice compared with uninfected controls (figure 2C). Contrasting the balanced immune phenotype observed in the stomach (figure 2C and online supplemental figure 2G), this was accompanied by a reduction in $Foxp3^+$ Treg cells (figure 2D and online supplemental figure 2G). Multiplexed ChipCytometry corroborated an overall reduction of Treg cells, and additionally revealed their compartmentalisation within the lamina propria in infected colonic tissue (figure 2E).

We next confirmed the specificity of these T cells for *H. pylori* by restimulating lamina propria $CD4^+$ T cells with *H. pylori* lysate and measuring the release of the pro-inflammatory cytokine IL-17A, which has been previously described to be one of the main players in the immune response to *H. pylori*.[1] A specific IL-17A/$CD4^+$ T cell response was observed in infected C57BL/6 and $Apc^{+/min}$ mice (online supplemental figure 2H).

To characterise in depth the specific intestinal immune response elicited by gastric *H. pylori*, we investigated the immune cell compartment on a single cell level by performing 10X single-cell RNA sequencing (scRNAseq) (dataset).[14] We isolated and sorted single $CD45^+$ immune cells of intestinal and colonic tissue from $Apc^{+/min}$ mice and littermate WT controls that had been infected for 12 weeks with *H. pylori*, and compared them with non-infected controls (online supplemental figure 2I).

Unsupervised clustering identified 16 clusters according to their transcriptional profiles, which are visualised using Uniform Manifold Approximation and Projection (UMAP)[15] (figure 2F and online supplemental figure 2J) and were annotated based on known marker genes (online supplemental figure 2K).

To further characterise the Treg cell compartment, we subclustered and annotated Treg cells, which resulted in three subclusters: activated Treg cells (act. Tregs); peripherally derived Treg cells (pTregs), characterised by high RORγt expression and thymus-derived Treg cells (tTregs), characterised by GATA3 expression[16 17] (figure 2G and online supplemental figure 2L). We then computed a Treg effector score[18] (figure 2H and online supplemental figure 1), and found significantly increased Th17 differentiation genes in infected act. Tregs (figure 2H and online supplemental table 1), indicating that *H. pylori* infection reprogrammes Treg cells into potentially pathogenic $Foxp3^+$ IL-$17A^+$ T cells.

Finally, to understand cell dynamics of T cells in infected mice, we calculated RNA velocity vectors, which predict future states of individual cells based on ratios of spliced and unspliced messenger RNAs.[19] In line with our previous findings, when looking at the CD4 clusters, it was apparent that less CD4 cells were projected towards CD4 Treg cells in infected *Apc* mice (online supplemental figure 2M).

In summary, our results show that *H. pylori* infection induces a *H. pylori*-specific pro-inflammatory immune response in the small intestine and colon of infected mice, that is characterised by loss of Treg cells and their differentiation into $Foxp3^+$ IL-$17A^+$ T cells.

Activation of carcinogenic signalling pathways and loss of goblet cells characterise the intestinal epithelial response to *H. pylori* infection

Considering the alterations induced by *H. pylori* in intestinal immune cells independently of adenomatous polyposis coli (*APC*) mutations in WT mice, we analysed the effect on signalling pathways putatively mediating the pro-carcinogenic effects of *H. pylori* infection in the epithelium. Therefore, we assessed transcriptomic profiles of $EPCAM^+$ epithelial cells from $Apc^{+/min}$ mice in our scRNAseq data (online supplemental figure 2I) (dataset).[14] Unsupervised clustering revealed 15 clusters according to their transcriptional profiles, which were visualised as UMAP (figure 3A and online supplemental figure 3A) and annotated based on known marker genes (online supplemental figure 3B).

Pseudo-spatial distribution of epithelial cells along the crypt-villus axis were computed to confirm correct annotation of cell types[20 21] (online supplemental figure 3C).

Here, we specifically explored signalling pathways associated with CRC initiation and development, namely STAT3 and NF-κB. Notably, these pathways also orchestrate key inflammatory mechanisms in inflammation-driven colon cancer and have been extensively related to *H. pylori* infection.[22–24] We computed a score of genes involved in the Jak-STAT signalling pathway, which revealed significantly higher scores in enterocytes of WT and $Apc^{+/min}$ mice upon *H. pylori* infection (figure 3B, online supplemental figure 3D and online supplemental table 1). Increased STAT3 signalling was only detected in stem cells of WT mice and not in $Apc^{+/min}$ mice upon *H. pylori* infection (online supplemental figure 3D), which can be linked to the binary role of STAT3 in tumourigenesis and a reduced availability of STAT3-inducing receptors during tumour progression, as we found a decreased expression of the IL-22 receptor *Il22ra1* on stem cells of *Apc* mutant mice upon *H. pylori* infection, but not in infected wt mice or in enterocytes (online supplemental figure 3E). When assessing NF-κB signalling in enterocytes, higher scores were observed upon *H. pylori* infection (online supplemental figure 3F and online supplemental figure 1).

As it has been shown that activation of epithelial STAT3 favours recruitment of lymphocytes, while inhibiting infiltration of Treg cells in the colon,[25] we confirmed hyperactivation of STAT3 in tissue samples from 24 weeks infected *H. pylori* WT (figure 3C) and *Apc* mutant mice (online supplemental figure 1A, figure 3D), which was accompanied by enhanced proliferation as detected by Ki67 staining (figure 3C).

Given that a functional intestinal barrier is depending on mucus replenishment by goblet cells, we next assessed their status by periodic acid-Schiff (PAS) staining. We observed reduced number of mucus producing cells in the small intestine and in the colon of *H. pylori*-infected WT (figure 3C) and *Apc* mutant mice (figure 3E) compared with uninfected controls.

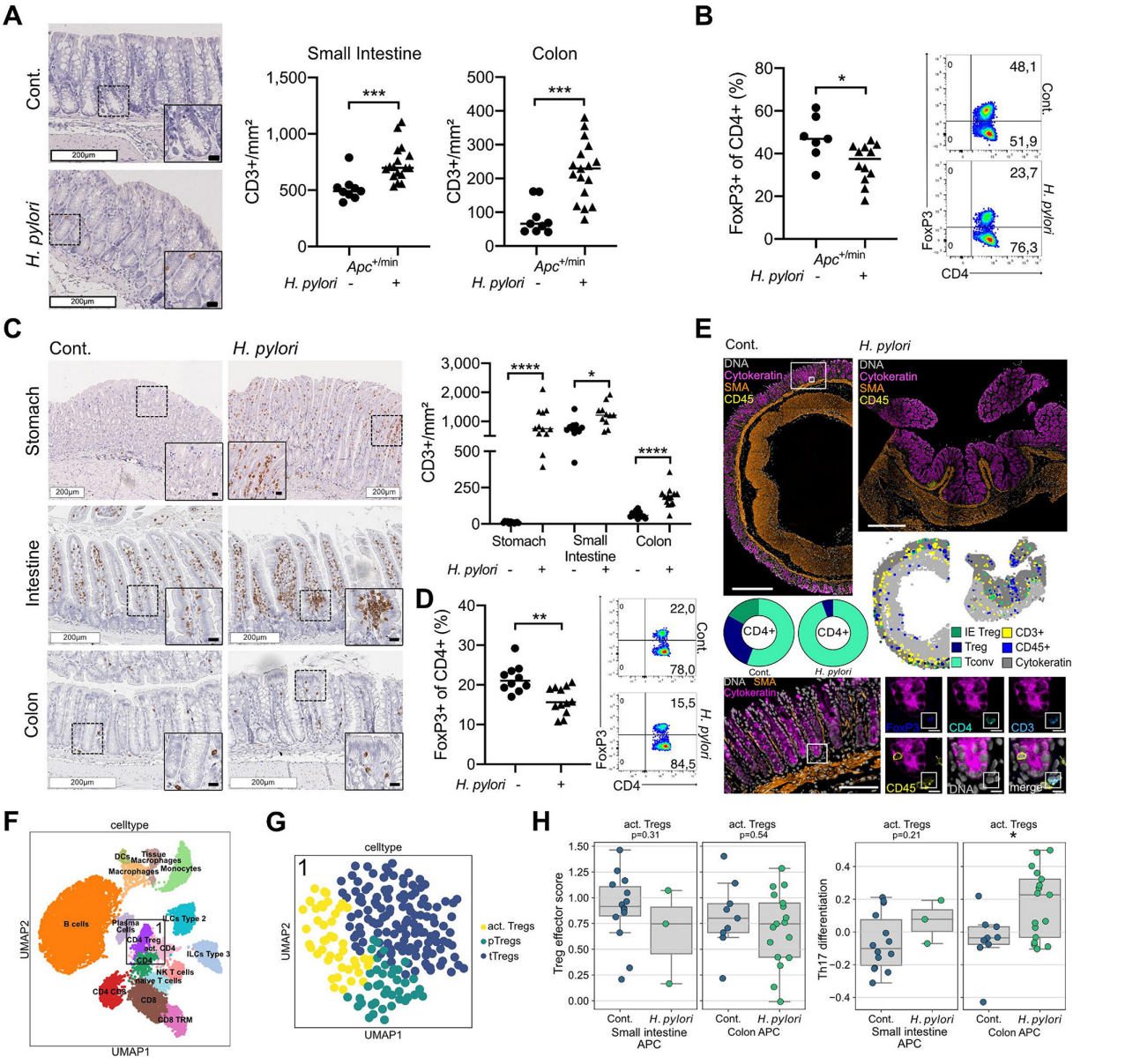

Figure 2 *Helicobacter pylori* infection induces a pro-inflammatory response in the intestine. (A) Representative pictures of colonic CD3+ stainings of *H. pylori*-infected and non-infected *Apc*$^{+/min}$ mice after 12 weeks of infection are shown. Squares highlight zoom in. White scale bars correspond to 200 µm, black scale bars to 20 µm. Quantification of positive cells per mm^2 small intestine and colon tissue is shown. Pooled data of three independent experiments. (B) Flow cytometric analysis of intestinal lamina propria lymphocytes isolated from *H. pylori*-infected and non-infected *Apc*$^{+/min}$ mice after 12 weeks of infection. Frequency of FoxP3+ cells of CD4+ T cells are shown, gated on live, single cells, CD45+ and CD3+. Pooled data of two independent experiments. (C) Representative CD3+ staining of stomach, small intestine and colon tissue sections of *H. pylori*-infected and non-infected C57BL/6 mice after 24 weeks of infection. Quantification of intraepithelial cells per mm^2 is shown. Squares highlight zoom in. White scale bars correspond to 200 µm, black scale bars to 20 µm. Pooled data of two independent experiments. (D) Frequency of FoxP3+ cells of CD4+ T cells are shown. Cells were gated on live, single cells, CD45+ and CD3+. Pooled data of two independent experiments. (E) Overview of colon tissue stained with multiplexed chip cytometry. Automatic image processing of multiplexed chip cytometry on colon tissue determines CD4+ T cell properties in *H. pylori*-positive and *H. pylori*-negative C57BL/6 mice. Frequencies of conventional T cells (Tconv), regulatory T cells (Treg) and intraepithelial regulatory T cells (IE Treg) are shown. Scale bar in overview corresponds to 500 µm. Representative picture of colon tissue stained with multiplexed chip cytometry. FoxP3+ cell, defined by intranuclear FoxP3+, CD4+CD3+ and CD45+ staining. Large scale bar corresponds to 100 µm, small scale bars to 10 µm. Representative data of one experiment. (F) Annotated immune cells plotted as Uniform Manifold Approximation and Projection (UMAP), clusters for further analysis are highlighted (1=CD4 Treg, 2=CD8 and CD8 TRM). (G) Unsupervised clustering and annotation of Treg cluster as UMAP, n=217 cells. act. Tregs, activated Tregs; pTregs, peripherally induced Tregs; tTregs, thymically derived Tregs. (H) Gene set score of Treg effector genes and Th17 differentiation genes, comparing activated Treg cells from small intestine and colon of *H. pylori*-infected and non-infected *Apc*$^{+/min}$ (APC) mice. Statistical significance was determined with Kruskal-Wallis test. Each symbol represents one animal/single cell, pooled from at least two independent experiments (n=6–10 mice/group/experiment) or two mice/group for single-cell data. Bars denote median. Unless otherwise specified, statistical significance was determined with Student's t-test in case of normal distribution, otherwise by Mann-Whitney U test, *p<0.05, **p<0.01, ***p<0.001, ****p<0.0001.

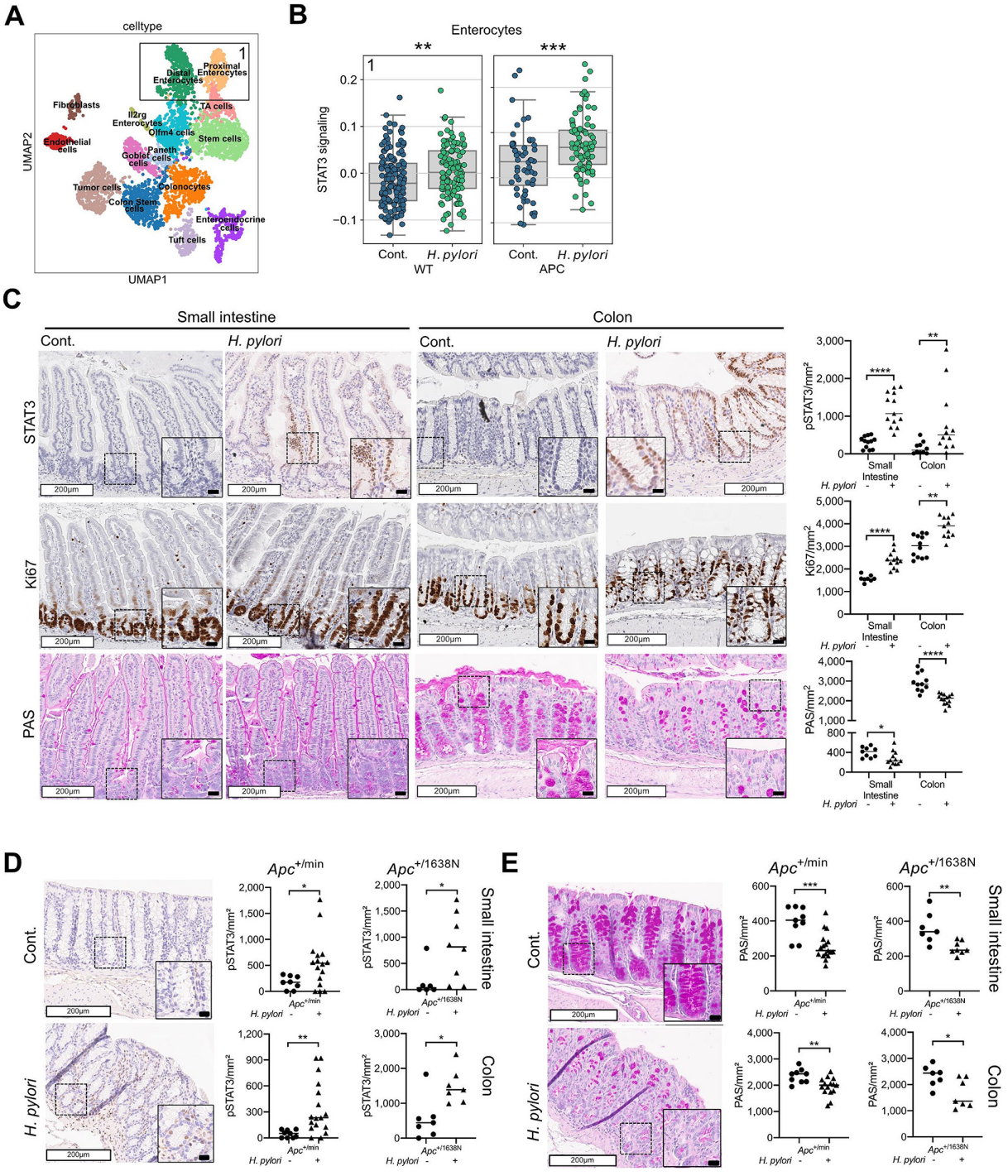

Figure 3 Activation of carcinogenic signalling pathways and loss of goblet cells characterise the intestinal epithelial response to *Helicobacter pylori* infection. (A) Annotated epithelial cells after unsupervised clustering plotted in Uniform Manifold Approximation and Projection (UMAP) space, n=2 mice per group, n=4249 cells. Clusters for further analysis are highlighted (1=enterocytes). (B) Gene set score of STAT3 signalling genes, comparing intestinal enterocytes from *H. pylori*-infected and non-infected $Apc^{+/+}$ (WT) and $Apc^{+/min}$ (APC) mice. Statistical significance was determined with Kruskal-Wallis test. (C) Representative pSTAT3, Ki67 and periodic acid-Schiff (PAS) staining of small intestine and colon tissue of *H. pylori*-infected and non-infected C57BL/6 mice. Quantification of positive cells per mm^2 is shown. Squares highlight zoom in. White scale bars correspond to 200 µm, black scale bars to 20 µm. Pooled data of two independent experiments. (D) Representative pictures of colonic pSTAT3 staining of *H. pylori*-infected and non-infected $Apc^{+/min}$ and $Apc^{+/1638N}$ mice are shown. Squares highlight zoom in. White scale bars correspond to 200 µm, black scale bars to 20 µm. Quantification of positive cells per mm^2 are shown. Pooled data of three independent experiments. (E) Representative pictures of colonic PAS staining of *H. pylori*-infected and non-infected $Apc^{+/min}$ and $Apc^{+/1638N}$ mice are shown. Squares highlight zoom in. White scale bars correspond to 200 µm, black scale bars to 20 µm. Quantification of positive cells per mm^2 are shown. Pooled data of three independent experiments. Each symbol represents one animal/single cell, pooled from at least two independent experiments (n=6–10 mice/group/experiment) or two mice/group for single-cell data. Bars denote median. Unless otherwise specified, statistical significance was determined with Student's t-test in case of normal distribution, otherwise by Mann-Whitney U test, *p<0.05, **p<0.01, ***p<0.001, ****p<0.0001.

To explore in depth the effects of *H. pylori* infection on the goblet cells, we clustered and annotated goblet cells in our scRNAseq dataset based on goblet cell differentiation markers.[26] This revealed immature, characterised by high expression of *Tff3*; intermediate, highly expressing *Oasis* and terminal goblet cells, with high expression of *Muc2* and *Klf4* (online supplemental figure 3G,H). Maturational states were distinctly affected by *H. pylori* infection, with a switch to less differentiated goblet cells (online supplemental figure 3I). To assess goblet cell functionality, we assessed the expression of genes encoding for antimicrobial peptides *Reg3b* and *Reg3g*, which are known to play a role in response to pathogens and inflammation[27] (online supplemental table 1). We found them to be reduced upon *H. pylori* infection (online supplemental figure 3J). As those genes are known to be downstream targets of STAT3, we checked for STAT3 signalling specifically in the goblet cell cluster, which was—in contrast to the increased STAT3 signalling in enterocytes and stem cells—not induced upon *H. pylori* infection (online supplemental figure 3K). These findings are consistent with a compromised intestinal barrier integrity induced by *H. pylori* infection, independent of *APC* status.

To explain the absolute loss of goblet cells we observed in infected mice, we studied cellular dynamics of goblet cells by means of RNA velocities. In the colon, we observed less directionality from the stem cell cluster towards the goblet cell cluster, and at the same time a higher projection towards the colonocyte cluster upon *H. pylori* infection (online supplemental figure 3J), in contrast to the small intestinal goblet cell cluster, where cell dynamics seem to be restricted to the goblet cell cluster itself. When assessing the expression of *Atoh1*, which is known to drive terminal differentiation into the secretory lineage,[28] in stem cells of both small intestine and colon, a signficiantly lower expression was found upon *H. pylori* infection (online supplemental figure 3K). These findings indicate a skewed differentiation of stem cells rather into unspecialised colonozytes than into goblet cells.

Together, these results indicate that *H. pylori* induces carcinogenic signalling pathways and has a detrimental impact on mucus-producing goblet cells in the small intestine and colon of WT and *Apc* mutant mice.

H. pylori infection favours the presence of mucus-degrading microbiota and shapes a pro-inflammatory and pro-carcinogenic microbiota signature

Microbiota alterations and aberrant presence of certain bacterial species in the small intestine have been related to the development of CRC.[29] This could be an additional mechanism by which *H. pylori* contributes to intestinal carcinogenesis, since *H. pylori* infection has been shown to alter microbiota signatures.[30] Therefore, we assessed to which extent *H. pylori* infection influenced small intestinal and colonic microbial composition by performing 16S RNA sequencing (dataset).[14] While we found significantly increased abundance of *Helicobacter* spp in the stomach of 24 weeks infected mice, we did not detect *H. pylori* in intestine and colon (online supplemental figure 4A). When comparing the microbiota in caecum and colon of infected and non-infected mice via taxonomic profiling, we observed apparent changes at phylum level upon *H. pylori* infection (figure 4A). Furthermore, we found signs of decreased α-diversity in small intestine upon *H. pylori* infection (online supplemental figure 4B) as well as significantly different β-diversity in caecum, stool and small intestine between non-infected and infected mice (online supplemental figure 4C). Differential abundance testing revealed *Akkermansia* spp to be enriched in 24 weeks infected WT mice (online supplemental figure 4D, figure 4B). When exploring the data for further species sharing the mucus-degrading characteristics of *Akkermansia* spp, we found an increase in *Ruminococcus* spp (figure 4B and online supplemental figure 4D). The abundance of both species was also higher in *Apc* mutant mice (online supplemental figure 1A) upon *H. pylori* infection (figure 4C,D).

To determine the functional effects of *H. pylori*-induced microbiota signatures independent of mutant APC, we performed a stool transfer experiment from infected and non-infected specific pathogen-free (SPF) mice into germ-free WT mice (online supplemental figure 4E). This revealed an increased T-cell infiltration into intestinal and colonic epithelia (figure 4E and online supplemental figure 4F), a reduction of $Foxp3^+$ Treg cells (figure 4F) and lower amounts of RORγt+ Treg cells (figure 4G), which are known to be microbiota-induced,[31] in WT stool recipients from *H. pylori*-infected mice. Furthermore, we observed enhanced STAT3 signalling in intestines of WT mice that received stool from *H. pylori*-infected mice (figure 4H and online supplemental figure 4G). In order to ultimately assess the contribution of *H. pylori*-induced changes in microbiota to intestinal carcinogenesis, we performed a further stool transfer experiment from SPF non-infected and *H. pylori*-infected $Apc^{+/1638N}$ mice and WT littermates into germ-free $Apc^{+/1638N}$ mice (online supplemental figure 4H). Higher tumour numbers in stool recipients from *H. pylori*-infected mice were found, which was already evident in WT mice and further enhanced in an $Apc^{+/1638N}$ background (online supplemental figure 4I).

Together, *H. pylori* alters the microbiota of the lower GI tract, favours mucus-degrading microbiota in both WT and *Apc* mutant mice and induces a pro-inflammatory and pro-carcinogenic microbiota signature.

H. pylori-induced colorectal carcinogenesis is prevented by eradication

The interplay between a pro-inflammatory response and activation of pro-carcinogenic signalling, accompanied by alterations in microbiota characterised *H. pylori*-driven intestinal tumourigenesis. To dissect the contribution of inflammation in the absence of microbiota, we infected $Apc^{+/1638N}$ mice under germ-free conditions (online supplemental figure 5A,B). We observed similar immune alterations as in SPF mice, namely increased $CD3^+$ T cell infiltration and reduction of Treg cells in small intestine and colon (figure 5A, online supplemental figure 5E,B). In contrast, germ-free mice barely showed activation of STAT3 signalling, and no reduction of goblet cells upon *H. pylori* infection (online supplemental figure 5C–E). Importantly, we did not observe significant differences in tumour number between control and *H. pylori*-infected germ-free $Apc^{+/1638N}$ mice (figure 5C), which, in combination with our findings from stool transfer experiments (figure 4 and online supplemental figure S4), indicates a strong contribution of *H. pylori*-induced changes in microbiota to the tumour phenotype, and suggests, that *H. pylori*-induced carcinogenesis in the small intestine and colon is a multifactorial process involving the interplay of the pro-inflammatory immune response, alterations in microbiota and pro-carcinogenic signalling. Therefore, we next sought to determine whether eradication of *H. pylori* infection could abrogate the carcinogenic process, by treating the mice with a triple therapy regimen consisting of clarithromycin, metronidazole and omeprazole,[32] reflecting the 'Italian triple therapy' regimen also used in infected patients to eradicate *H. pylori* (figure 5D and online supplemental figure 5F). Importantly, we

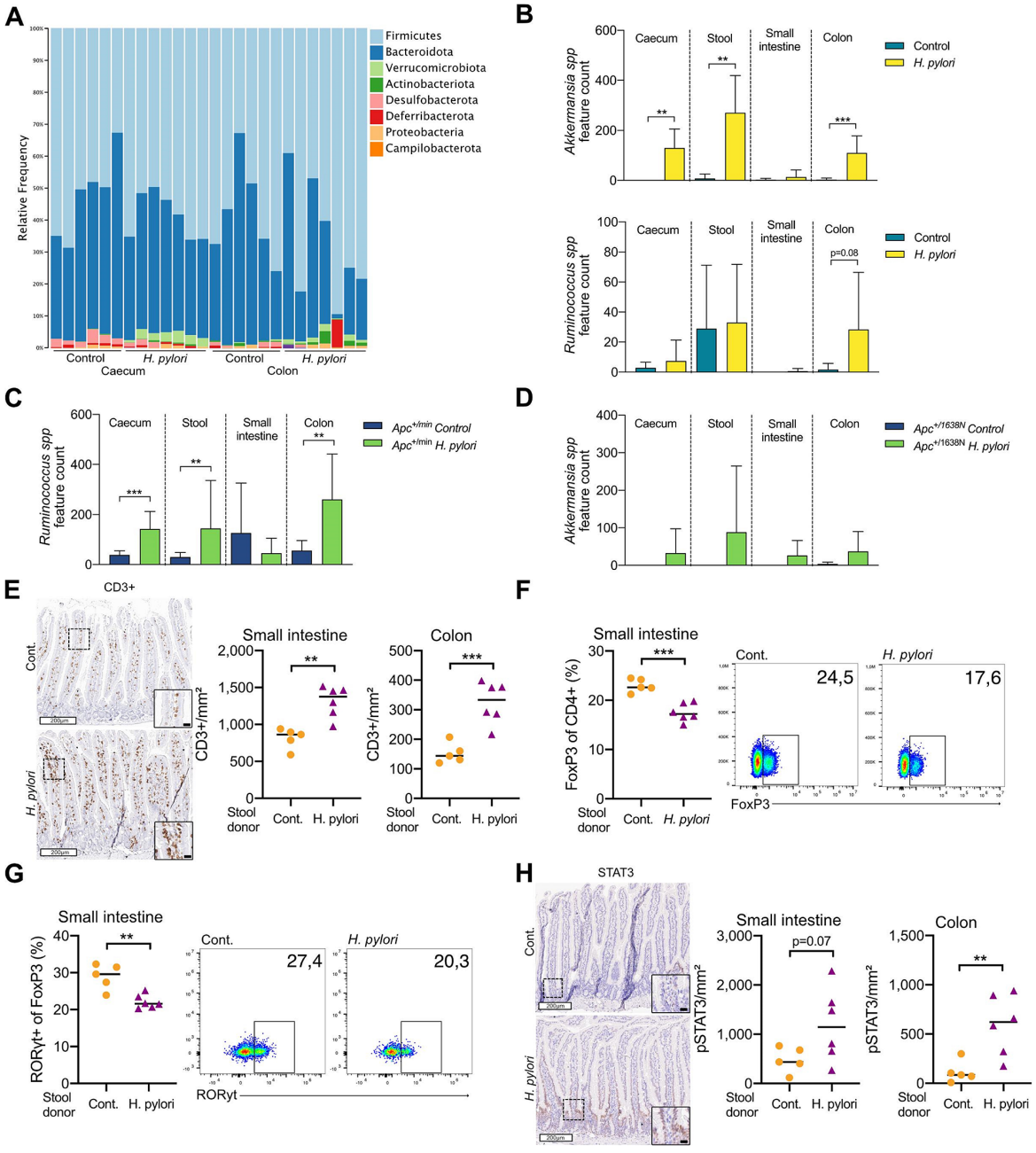

Figure 4 *Helicobacter pylori* infection favours the presence of mucus-degrading microbiota and shapes a pro-inflammatory and pro-carcinogenic microbiota signature. (A) Relative taxonomic frequencies on phyla level in 16S rRNA sequenced caecum and colon samples of *H. pylori*-infected and non-infected C57BL/6 mice (n=6–8 mice/group). Data of one representative experiment of two to three independent experiments. (B) Feature counts of Amplicon Sequence Variants (ASVs) of *Akkermansia* spp and *Ruminococcus* spp in ceacum, stool, small intestine and colon of *H. pylori*-infected and non-infected C57BL/6 mice (n=6–8 mice/group). Data of one representative experiment of two to three independent experiments. (C) Feature counts (ASVs) of *Ruminococcus* spp of ceacum, stool, small intestine and colon of *H. pylori*-infected and non-infected *Apc*$^{+/min}$ mice (n=4–5 mice/group). Data of one representative experiment of two to three independent experiments. (D) Feature counts (ASVs) of *Akkermansia* spp of ceacum, stool, small intestine and colon of *H. pylori*-infected and non-infected *Apc*$^{+/1638N}$ mice (n=4–5 mice/group). Data of one representative experiment of two to three independent experiments. (E) Representative pictures of intestinal CD3+ stainings of germ-free wild-type (WT) mice receiving stool transfer from *H. pylori*-infected (*H. pylori*) and non-infected (*Cont.*) WT mice analysed 12 weeks after transfer are shown. Squares highlight zoom in. White scale bars correspond to 200 µm, black scale bars to 20 µm. Quantification of positive cells per mm^2 small intestine and colon tissue is shown. Data of one experiment. (F) Flow cytometric analysis of intestinal lamina propria lymphocytes isolated from germ-free WT mice receiving stool transfer from *H. pylori*-infected (*H. pylori*) and non-infected (*Cont.*) WT mice analysed 12 weeks after transfer. Frequency of FoxP3+ cells of CD4+ T cells and (G) RORγt+ cells of FoxP3+ T cells are shown, gated on live, single cells, CD45+, CD3+ and CD4+. Data of one experiment. (H) Representative pictures of intestinal STAT3+ stainings of germ-free WT mice receiving stool transfer from *H. pylori*-infected (*H. pylori*) and non-infected (*Cont.*) WT mice analysed 12 weeks after transfer are shown. Squares highlight zoom in. White scale bars correspond to 200 µm, black scale bars to 20 µm. Quantification of positive cells per mm^2 small intestine and colon tissue is shown. Data of one experiment. Data shown as bars with mean and SD or each symbol represents one animal (n=5–6 mice/group). Bars denote median. Statistical significance was determined with Student's t-test in case of normal distribution, otherwise by Mann-Whitney U test, **p<0.01, ***p<0.001.

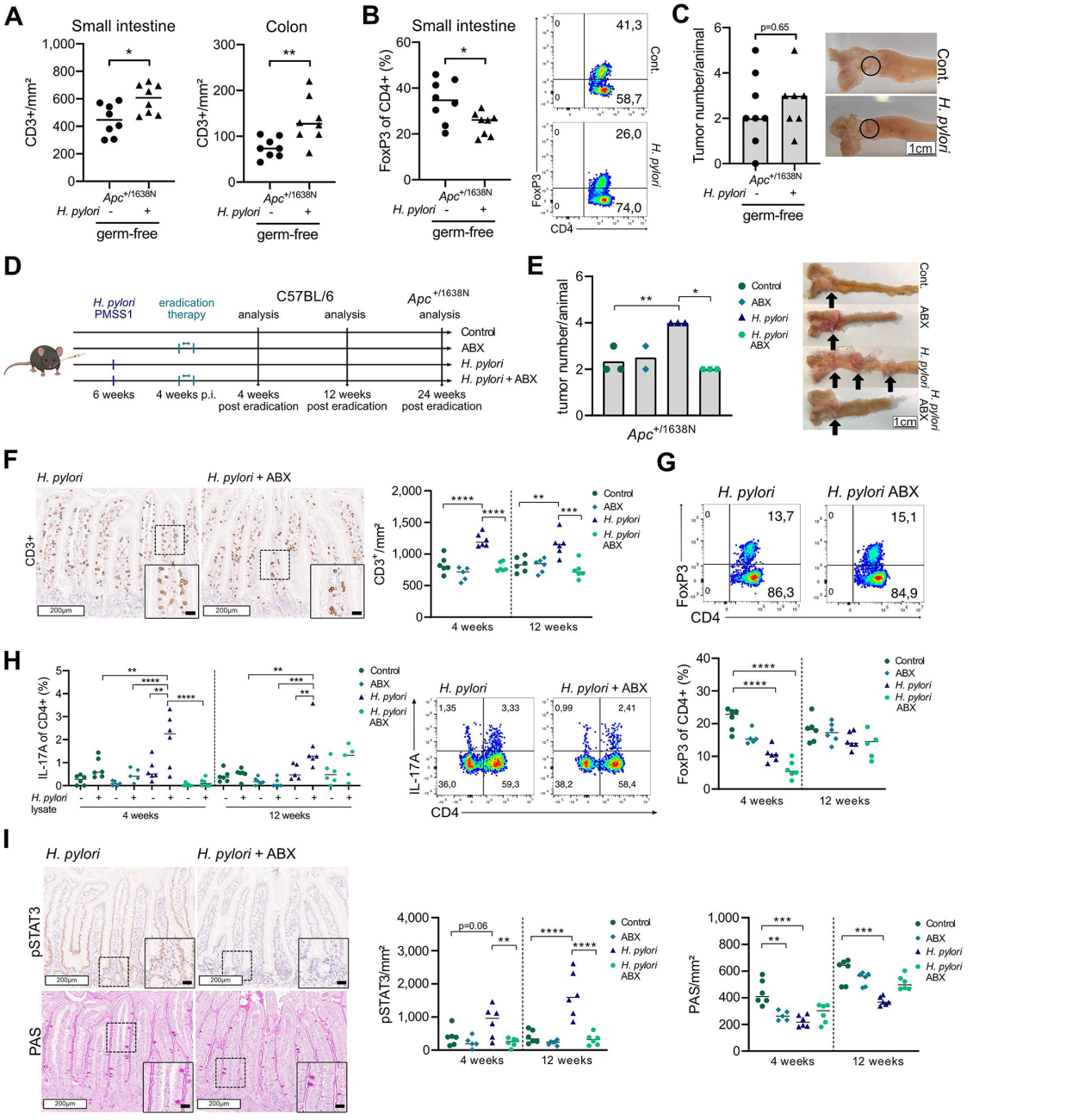

Figure 5 *Helicobacter pylori*-induced intestinal carcinogenesis is prevented by eradication. (A) Quantification of small intestinal and colonic intraepithelial CD3+ cells per mm^2 of *H. pylori*-infected and non-infected germ-free *Apc*$^{+/1638N}$ mice is shown. Pooled data of two independent experiments (n=8 mice/group). (B) Frequencies of FoxP3+ cells of CD4+ T cells, gated on live, single cells, CD45+ and CD3+ of *H. pylori*-infected and non-infected germ-free *Apc*$^{+/1638N}$ mice are included. Representative pseudo-colour plots are shown. Pooled data of two independent experiments (n=8 mice/group). (C) Intestinal tumour counts of *H. pylori*-infected and non-infected germ-free *Apc*$^{+/1638N}$ mice and representative pictures of tumours (circled) are shown (n=8 mice/group). (D) Experimental setup of *H. pylori* eradication therapy of C57BL/6 and *Apc*$^{+/1638N}$ mice. (E) Tumour counts of non-infected, antibiotically treated, *H. pylori*-infected and *H. pylori*-eradicated *Apc*$^{+/1638N}$ mice and representative pictures of tumours in the small intestine. Data of one experiment (n=2–3 mice/group). (F) Representative pictures of CD3+ stainings from small intestinal tissue of *H. pylori*-infected and *H. pylori*-eradicated C57BL/6 mice are shown. Squares highlight zoom in. White scale bars correspond to 200 µm, black scale bars to 20 µm. Quantification of positive cells per mm^2 is shown. Data of one experiment (n=5–6 mice/group). (G) Flow cytometric analysis of intestinal lamina propria lymphocytes reveals frequency of FoxP3+CD4+ T cells, gated on live, single cells, CD45+ and CD3+. Data of one experiment (n=5–6 mice/group). (H) Flow cytometric analysis of intestinal lamina propria lymphocytes reveals IL-17A release of CD4+ T cells, restimulated with whole *H. pylori* lysate. Cells are gated on live, single cells, CD45+ and CD3+. Data of one experiment (n=5–6 mice/group). (I) Representative pictures of pSTAT3 and periodic acid-Schiff (PAS) staining from intestinal tissue of *H. pylori*-infected and *H. pylori*-eradicated C57BL/6 mice are shown. Squares highlight zoom in. White scale bars correspond to 200 µm, black scale bars to 20 µm. Quantification of positive cells per mm^2 is shown. Data of one experiment (n=5–6 mice/group). Each symbol represents one animal. Bars denote median. Statistical significance between two groups was determined with Student's t-test in case of normal distribution and otherwise with Mann-Whitney U test. Among more than two groups, ordinary one-way analysis of variance with Tukey's multiple comparisons test was applied in case of normal distribution, otherwise Kruskal-Wallis test with Dunn's multiple comparisons test, *p<0.05, ***p<0.001.

found that after antibiotic eradication, tumour burden was at the same levels as in uninfected controls (figure 5E). To delineate that the underlying changes in the intestinal immune response were directly induced by *H. pylori* infection and independent of mutated *Apc*, we analysed the effect of *H. pylori* eradication on C57Bl/6 mice (figure 5D and online supplemental figure 5F), and found a lower $CD3^+$ T cell infiltration in the stomach (online supplemental figure 5G), small intestine and colon (figure 5F, online supplemental figure 5E) compared with infected mice at 4 and 12 weeks posteradication. The percentage of Treg cells was initially reduced in eradicated mice 4 weeks after treatment, while 12 weeks post-treatment, the percentage of $FoxP3^+$ T cells was observed to recover (figure 5G). A specific IL-17A/$CD4^+$ T cell response was observed in infected mice, which was initially lost after eradication therapy, but then reappeared after longer recovery time (figure 5H), supporting the specificity of the response to *H. pylori*, based on the given antigen encounter and response also in eradicated mice. Importantly, the clearance of infection resulted in normalisation of STAT3 activation and the number of PAS-positive cells (figure 5I and online supplemental figure 5H), confirming that *H. pylori* is specifically responsible for these changes.

In summary, our results demonstrate that *H. pylori* directly enhances colon carcinogenesis by shaping intestinal and colonic immune responses and inducing profound changes in intestinal/colonic microbiota and epithelial homeostasis. Eradication of *H. pylori* infection prevents its tumour-promoting effects also in the colon, providing a possible additional strategy to reduce CRC burden.

H. pylori alters colonic homeostasis in human

Our mouse models showed that *H. pylori* affects intestinal and colonic homeostasis at different cellular and molecular levels, which can ultimately enhance tumour development. To determine whether these effects were also observed in humans, we analysed immune signatures in a cohort of 154 human colon tissue samples (online supplemental table 2). Based on immune responses and histology of the stomach, we stratified samples according to *H. pylori* status into currently (actively) infected and eradicated patients. We found that *H. pylori*-actively infected as well as eradicated individuals showed higher infiltration of $CD3^+$ T cells in the colon compared with uninfected subjects (figure 6A). Using endoscopy-derived colon biopsies, we further characterised T cell responses by flow cytometry, which revealed tendencies towards more $CD3^+$ T cells in the colonic mucosa of currently infected patients (online supplemental figure 6A). In contrast, $CD4^+$ and $CD8^+$ subsets were not affected by *H. pylori* status (online supplemental figure 6B). Notably, the number of $FoxP3^+$ cells in the colonic mucosa was lowest in the currently infected group, whereas eradicated patients seem to level with negative controls (figure 6C). The overall loss of Tregs was confirmed via ChipCytometry (figure 6B), which additionally showed that intraepithelial localisation of Tregs is almost lost in colon samples from *H. pylori*-infected individuals (figure 6B and online supplemental figure 6C).

We next focused on the epithelial compartment and, in concordance with our findings in mice and our eradication experiments, found a higher number of pSTAT3-positive epithelial cells and a concomitant loss of mucus-producing cells in the colon of currently infected subjects, which was attenuated in eradicated patients (figure 6A).

Finally, we assessed microbial changes in stool of patients and found a difference in β-diversity between actively *H. pylori*-infected and *H. pylori*-negative patients ($p=0.062$), but not between *H. pylori*-eradicated and *H. pylori*-negative patients ($p=0.552$) (figure 6D). In contrast, we neither detected significant changes in α-diversity (online supplemental figure 6D) nor in Firmicutes-to-Bacteroidetes ratio (online supplemental figure 6E) between the three groups. Comparative microbiome profiling revealed Prevotellaceae and Peptostreptococcales, which have been associated with CRC, to be differentially abundant in *H. pylori*-positive patients (online supplemental figure 6F,G).

These results confirm that the immune and epithelial signatures identified in mouse models upon *H. pylori* infection are also observed in humans, and are accompanied by changes in microbiota compositions, which can further contribute to colon carcinogenesis. Furthermore, the attenuated phenotype observed in *H. pylori*-eradicated patients further supports *H. pylori* status as an independent risk factor for CRC and simultaneously offers an option for CRC prevention for those patients at risk.

DISCUSSION

Although selectively colonising the stomach, chronic *H. pylori* infection is associated with several extragastric diseases.[33] Epidemiological data indicate an association between *H. pylori* infection and a higher risk and aggressiveness of CRC, with an OR of 1.9,[34] an OR higher than for most other known risk factors, such as smoking, alcohol and body mass index.[34] However, these epidemiological data have not yet been confirmed experimentally, and a molecular mechanism by which *H. pylori* may promote CRC remained elusive. We employed *Apc* mutant mouse lines ($Apc^{+/min}$ and $Apc^{+/1638N}$) as surrogate models for human CRC, and observed a nearly twofold increase in tumour numbers in mice infected with *H. pylori*, which coincides with the OR observed in epidemiological studies. Remarkably, this increase was observed in the small intestine, where both models usually show most tumours, and was especially evident in the colon. This prompted us to decipher the potential mechanisms driving *H. pylori*-induced carcinogenesis in the small intestine and colon.

The effects of *H. pylori* infection on other organs are best understood for the lung, where chronic *H. pylori* infection imposes a regulatory immune signature that protects from asthma disease.[35] In contrast to these observations, we observed an *H. pylori* antigen-specific pro-inflammatory Th17-mediated response in the small intestine and colon, which was not balanced by an increase in Treg cells, as it occurs in the stomach or lung. The immune response mounted towards *H. pylori* originates from Peyer's patches in the gut,[2] which may explain why *H. pylori*-specific T cells also homed to intestinal and colonic mucosal sites. Interestingly, IL-17 was found to be increased in *H. pylori*-positive patients with gastritis and gastric cancer,[36] and in CRC, where Th17 signatures, including RORC, IL17, IL23 and STAT3, were linked to poorer prognosis.[37] Still, it was surprising to observe a loss of intestinal Treg cells, which also contrasts the balanced immune response usually observed in the stomach upon *H. pylori* infection. Additionally, we found that in the lower GI tract, Tregs were reprogrammed to upregulate Th17 differentiation markers. Murine and human studies have demonstrated that Treg cells can be reprogrammed to a distinct population, $Foxp3^+$/$IL17^+$ T cells, phenotypically and functionally resembling Th17 cells.[38] Particularly in CRC, the presence of $Foxp3^+$/$IL17^+$ T cells has been reported to be increased in the mucosa and peripheral blood of patients with chronic colitis as well as in colorectal tumours.[39] $Foxp3^+$/$IL17^+$ cells were shown to promote the development of tumour-initiating cells by increasing the expression of several CRC-associated markers

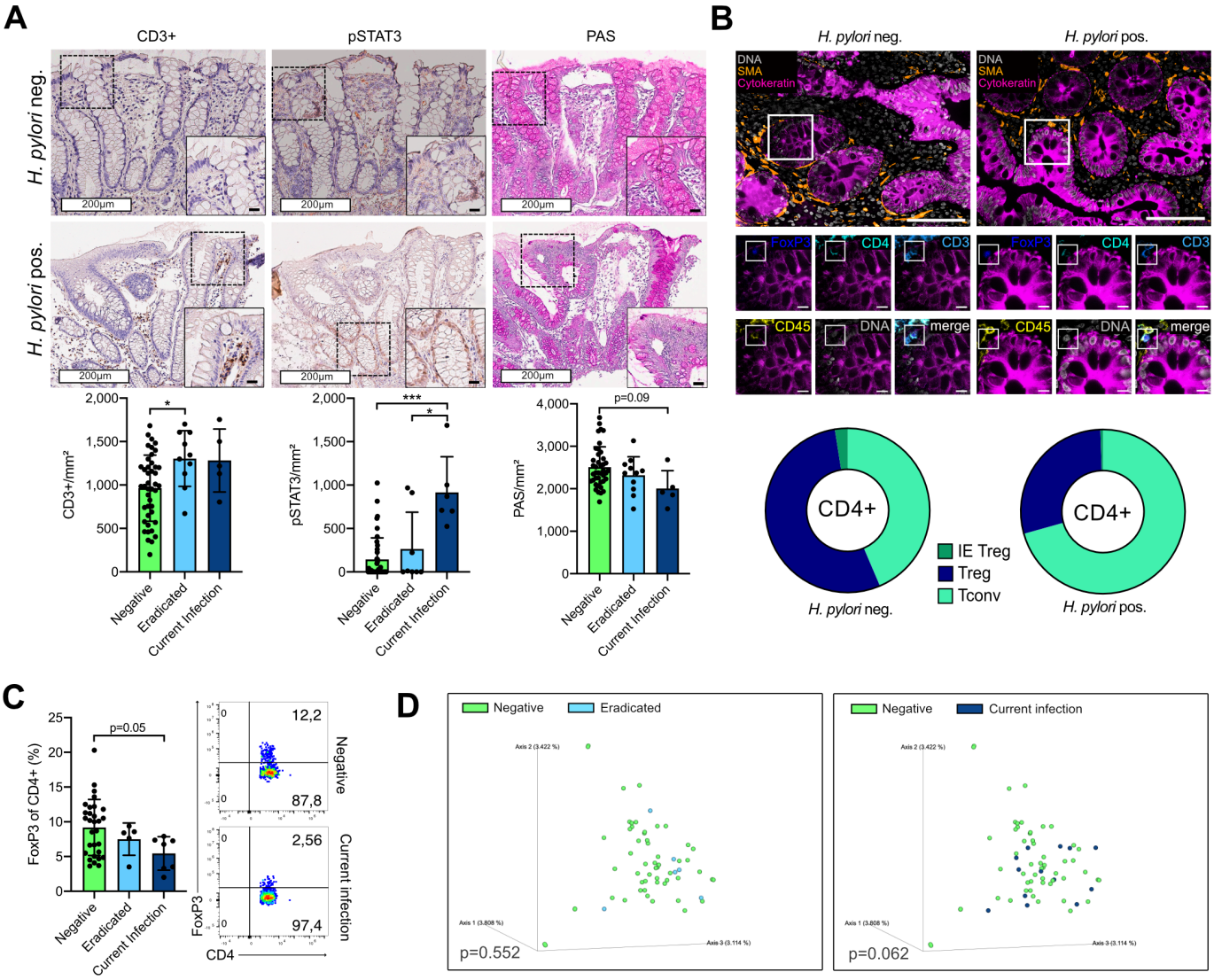

Figure 6 *Helicobacter pylori* alters colonic homeostasis in human. (A) Representative H&E, CD3+, pSTAT3 and periodic acid-Schiff (PAS) pictures of colonic tissue from *H. pylori* currently infected, eradicated and non-infected patients are shown. Squares highlight zoom in. White scale bars correspond to 200 µm, black scale bars to 20 µm. Quantification of total CD3+, intraepithelial STAT3 and PAS-positive cells per mm^2 are shown. (B) Representative pictures of human colon tissue stained by multiplexed chip cytometry. FoxP3+ cell, defined by intranuclear FoxP3+, CD4+, CD3+ and CD45+ staining are shown for *H. pylori*-negative and *H. pylori*-positive tissue. Large scale bar corresponds to 100 µm, small scale bar to 10 µm. Automatic image processing of multiplexed chip cytometry on colon tissue determines CD4+ T cell properties in *H. pylori*-positive and *H. pylori*-negative individuals: frequencies of conventional T cells (Tconv), regulatory T cells (Treg) and intraepithelial regulatory T cells (IE Treg) are shown. (C) Flow cytometric analysis of colon biopsies from *H. pylori* currently infected, eradicated and non-infected patients were conducted. Frequencies of FoxP3+ cells of CD4+ T cells, gated on live, single cells, CD45+ and CD3+ are shown and representative pseudo-colour plots of *H. pylori* currently infected and negative individuals are included. (D) Bray-Curtis dissimilarity depicting β-diversity between *H. pylori*-infected and eradicated as well as *H. pylori*-infected and non-infected patients. Statistical significance was determined with permutational multivariate analysis of variance (PERMANOVA). Each symbol represents one patient, shown as bars with mean and SD. Statistical significance was determined with ordinary one-way analysis of variance with Tukey's multiple comparisons test in case of normal distribution, otherwise by Kruskal-Wallis test with Dunn's multiple comparisons test. *P<0.05, **p<0.01, ***p<0.001, ****p<0.0001.

such as CD44 and epithelial cell adhesion molecule EPCAM in bone marrow-derived mononuclear cells.[40] Thus, the pro-inflammatory Th17 response elicited by *H. pylori*, especially the differentiation of Treg cells to a Th17 phenotype, may constitute one of the major mechanisms enhancing tumour development. This is in line with literature showing that altered T cell homeostasis is a key event during colorectal carcinogenesis, driving tumour development and progression, and determining treatment response of patients with CRC.[41]

Mutations in the gene encoding *APC* are the most frequent driver mutations leading to sporadic CRC, together with mutations in *TP53* and *KRAS*.[42 43] Pro-inflammatory and proliferative signalling pathways such as STAT3, NF-κB and WNT signalling, activated by signals derived from epithelial and immune cells, drive chronic inflammation, a known mechanism contributing to CRC.[24 44] CRC risk is markedly increased in patients with chronic inflammatory bowel disease, with the risk rising with the duration of disease, from 8.3% after 20 years, to 18.4% after

30 years.[45] Mechanistically, besides immune signalling by Th17 cells, activation of pro-inflammatory signalling pathways as well as altered microbiota, contribute to the pathogenesis of colitis-associated cancer.[46]

The strong pro-inflammatory response induced locally by *H. pylori* in the small intestine was accompanied by the activation of NF-κB and STAT3 pathways. Activation of STAT3 signalling has been strongly related to tumour initiation and development and progression, while levels of activated STAT3 in the tissue correlate with tumour invasion, tumour, node, metastases stage and reduced overall survival of patients with CRC.[47] In addition, the activation of epithelial STAT3 was reported to downregulate the expression of chemokines important for the recruitment of Treg cells in the intestine.[25] Therfore, it is tempting to speculate that during *H. pylori* infection, activation of STAT3 in intestinal and colonic epithelial cells contributes to loss of Treg recruitment, thereby supporting malignant transformation of the intestinal tissue. This central role for STAT3 during carcinogenesis in the intestine is supported by the fact that depletion of STAT3 in $Apc^{+/min}$ mice led to a reduction in the incidence of early adenomas.[48] Furthermore, in $Apc^{+/min}$ mice, tumour progression and metastasis were characterised by loss of STAT3 signalling in stem cells due to lower IL-22-receptor expression.[48 49] We observed similar characteristics in our *H. pylori*-infected mice, indicative of more advanced tumourigenesis.

Importantly, we observed a reduction and normalisation of STAT3 levels after eradication of *H. pylori*, which resulted in a normalisation of tumour load. Notably, for eradication, a treatment regimen also applied in humans was used in order to be able to translate the results to humans.

The function of STAT3 as oncogene or tumour suppressor seems to be determined by the milieu eliciting its activation as well as the local gut microbiota,[50] which is increasingly recognised as an important regulator of colonic cancer development.[51] Interestingly, microbial induction of IL-17A production has been shown to endorse colon cancer initiation and progression in $Apc^{+/min}$ mice, which was mediated via STAT3 signalling.[52] We thus hypothesised that alterations in microbiota compositions in the intestine and colon induced by *H. pylori* may also contribute to carcinogenesis.[30 53] Indeed, when housing mice under germ-free conditions, activation of STAT3 and tumour development were lower upon *H. pylori* infection, but not completely normalised, indicating that microbiota alterations are involved in the phenotype but not exclusively responsible.

Such disturbances in gut microbiota communities have been shown to contribute to CRC development and progression.[29] *H. pylori* is known to affect local gastric microbiota, and distant microbial populations in intestine and colon.[30 54] It has been shown that inflammation-driven dysregulation of microbiota can promote colorectal tumour formation and progression[55] and that in response to bacterial stimuli or pathogen-associated molecular receptors, pro-inflammatory pathways such as c-Jun/JNK and STAT3 signalling pathways are activated and accelerate intestinal tumour growth in $Apc^{+/min}$ mice.[50] This was supported by our findings from transferring stool of *H. pylori*-infected SPF mice into germ-free mice, which led to lower abundance of FoxP3+ Treg cells and microbiota-induced (FoxP3+RORγt+) Treg cells as well as STAT3 induction in recipients of stool from *H. pylori*-infected mice, and eventually an accelerated tumour development in comparison to stool transferred from non-infected mice. Together, these data indicate that *H. pylori*-induced pro-inflammatory and pro-carcinogenic microbial signatures are involved in and indispensable to promote intestinal tumour growth.

Our data revealed a distinct mucus-degrading microbiota signature associated with *H. pylori* infection in mice, namely enrichment with *Akkermansia* spp and *Ruminococcus* spp, while in human samples from *H. pylori*-infected patients, bacterial taxa associated with CRC, Prevotellaceae and Peptostreptococcales, were found.[29] Although some studies established an inverse correlation between the presence of *Akkermansia* and GI diseases,[56] *Akkermansia* has been reported to be increased in patients with CRC most likely due to the overexpression of certain mucins in the tumours.[57] Notably, we also observed a general loss of goblet cells, which are important to produce mucins and antimicrobial peptides. This loss of goblet cells was also observed in clinical samples from *H. pylori*-infected patients undergoing colonoscopy. Thus, *H. pylori* infection disrupts, by two distinct mechanisms, intestinal mucus integrity essential to maintain a healthy barrier to impair bacterial penetration. In the absence of a sufficient regulatory T cell response—as observed here—which normally keeps inflammatory signals at bay, the carefully balanced homeostasis maintained in the gut by the interplay of a 'healthy' microbiome and an intact mucosa then fails to balance the pro-inflammatory signature elicited by *H. pylori* infection, enabling carcinogenesis. Eradication of *H. pylori* restored intestinal homeostasis with reappearance of goblet cells and normalised the intestinal immune signature, which then completely abrogated the tumour-promoting effect.

Importantly, when analysing colonic biopsies from *H. pylori*-infected patients, we could observe the very same alterations as seen in mice, with activation of pro-carcinogenic signalling pathways and a significant reduction in Treg cells, and an increase of $CD3^+$ cells. The attenuated phenotype in eradicated patients highlight the clinical relevance of our findings and indicate that *H. pylori* infection is more than a mere risk factor for colon carcinogenesis, but actively promotes a pro-carcinogenic niche in the colon that may be prevented by eradication of *H. pylori*, which therefore could decrease the risk of CRC development in infected individuals. However, studies showing a correlation between *H. pylori* infection and CRC did not address the effect of antibiotic therapy. The inclusion of such cohorts in future studies is important to determine the impact of *H. pylori* eradication in CRC development.

In summary, our study provides solid experimental evidence that *H. pylori* infection accelerates intestinal and colonic tumour development, and offers insight into the underlying mechanisms. We suggest *H. pylori* screening and eradication as a potential measure for CRC prevention strategies.

Author affiliations
[1]Institute for Medical Microbiology, Immunology and Hygiene, School of Medicine, Technical University of Munich, Munich, Germany
[2]Boehringer Ingelheim Pharma GmbH & Co. KG, Drug Discovery Sciences, Biberach an der Riß, Germany
[3]Department of Surgery, Klinikum rechts der Isar, School of Medicine, Technical University of Munich, Munich, Germany
[4]Klinik und Poliklinik für Innere Medizin II, Klinikum rechts der Isar, School of Medicine, Technical University of Munich, Munich, Germany
[5]Institute of Pathology, Klinikum Bayreuth, Friedrich-Alexander University Erlangen-Nuremberg, Bayreuth, Germany
[6]Klinik für Innere Medizin II, Universitätsklinikum Freiburg, Freiburg, Germany
[7]Chair of Nutrition and Immunology, Technical University of Munich, Freising, Germany
[8]ZIEL Institute for Food & Health, Technical University of Munich, Munich, Germany
[9]Munich Partner Site, German Center for Infection Research (DZIF), Munich, Germany
[10]Institute of Virology, Helmholtz Center Munich - German Research Center for Environmental Health, Neuherberg, Germany
[11]Chair for Preventions of Microbial Diseases, School of Life Sciences, Technical University of Munich, Freising, Germany

Acknowledgements We thank members of the laboratory 'Chronic inflammation and carcinogenesis' for experimental help as well as critical discussion, with special thanks to Maximilian Koch, Karin Taxauer, Martin Skerhut and Teresa Burrell for experimental support. We thank Julia Horstmann and the team of the ColoBAC study at the Klinik und Poliklinik für Innere Medizin II, Klinikum rechts der Isar, for the supply of human biopsies. We thank Core Facility Microbiome of the ZIEL Institute for Food & Health, Technical University of Munich, for 16S rRNA sequencing services, as well as Dharmesh Singh and Nyssa Cullin. We thank Core Facility Gnotobiology of the ZIEL Institute for Food & Health, Technical University of Munich, for germ-free mice.

Contributors AR, RM-L and MG conceived the study. AR, AD and RM-L designed and analysed experiments. SJ contributed and provided code and support to single cell RNA sequencing and chip cytometry. VE and AW contributed to experiments. SJ and DHB provided methodological expertise. AD, SJ, RM-L and DHB contributed to data interpretation. MV, MM and MQ provided human biopsies. KPJ provided mouse models and critically revised the article. DH, DHB and LD critically revised the article. AR and RM-L wrote the article. AR, RM-L and MG revised the article. MG acquired the funding and is the guarantor of the article. All authors read and reviewed the article.

Funding This work was funded by the Deutsche Forschungsgemeinschaft (DFG (German Research Foundation)) SFB1371/1-395357507 (project P09 and project P04).

Competing interests None declared.

Patient and public involvement Patients and/or the public were not involved in the design, or conduct, or reporting, or dissemination plans of this research.

Patient consent for publication Not applicable.

Ethics approval This study was approved by Klinikum rechts der Isar #322/18Klinikum Bayreuth #241_20Bc. Participants gave informed consent to participate in the study before taking part.

Provenance and peer review Not commissioned; externally peer reviewed.

Data availability statement Data are available in a public, open access repository. Data are available on reasonable request. Raw single cell RNA sequencing and 16S rRNA sequencing data have been deposited with links to BioProject accession number PRJNA808836 in the NCBI BioProject database (https://www.ncbi.nlm.nih.gov/bioproject/PRJNA808836/).

ORCID iDs
Klaus Peter Janssen http://orcid.org/0000-0002-4707-7887
Michael Quante http://orcid.org/0000-0002-8497-582X
Dirk Haller http://orcid.org/0000-0002-6977-4085
Raquel Mejías-Luque http://orcid.org/0000-0002-4602-4927
Markus Gerhard http://orcid.org/0000-0001-9110-3950

REFERENCES

1 Shi Y, Liu X-F, Zhuang Y, *et al*. Helicobacter pylori-induced Th17 responses modulate Th1 cell responses, benefit bacterial growth, and contribute to pathology in mice. *J Immunol* 2010;184:5121–9.
2 Nagai S, Mimuro H, Yamada T, *et al*. Role of Peyer's patches in the induction of Helicobacter pylori-induced gastritis. *Proc Natl Acad Sci U S A* 2007;104:8971–6.
3 Censini S, Lange C, Xiang Z, *et al*. Cag, a pathogenicity island of Helicobacter pylori, encodes type I-specific and disease-associated virulence factors. *Proc Natl Acad Sci U S A* 1996;93:14648–53.
4 Stein M, Rappuoli R, Covacci A. Tyrosine phosphorylation of the Helicobacter pylori CagA antigen after cag-driven host cell translocation. *Proc Natl Acad Sci U S A* 2000;97:1263–8.
5 Mejías-Luque R, Zöller J, Anderl F, *et al*. Lymphotoxin β receptor signalling executes helicobacter pylori-driven gastric inflammation in a T4SS-dependent manner. *Gut* 2017;66:1369–81.
6 Oertli M, Sundquist M, Hitzler I, *et al*. DC-derived IL-18 drives treg differentiation, murine helicobacter pylori-specific immune tolerance, and asthma protection. *J Clin Invest* 2012;122:1082–96.
7 Kaebisch R, Mejías-Luque R, Prinz C, *et al*. Helicobacter pylori cytotoxin-associated gene a impairs human dendritic cell maturation and function through IL-10-mediated activation of STAT3. *J Immunol* 2014;192:316–23.
8 Kao JY, Zhang M, Miller MJ, *et al*. Helicobacter pylori immune escape is mediated by dendritic cell-induced Treg skewing and Th17 suppression in mice. *Gastroenterology* 2010;138:1046–54.
9 Oertli M, Noben M, Engler DB, *et al*. Helicobacter pylori γ-glutamyl transpeptidase and vacuolating cytotoxin promote gastric persistence and immune tolerance. *Proc Natl Acad Sci U S A* 2013;110:3047–52.
10 Chen C-C, Liou J-M, Lee Y-C, *et al*. The interplay between *helicobacter pylori* and gastrointestinal microbiota. *Gut Microbes* 2021;13:1–22.
11 Lofgren JL, Whary MT, Ge Z, *et al*. Lack of commensal flora in Helicobacter pylori-infected INS-GAS mice reduces gastritis and delays intraepithelial neoplasia. *Gastroenterology* 2011;140:210–20.
12 Gravina AG, Zagari RM, De Musis C, *et al*. Helicobacter pylori and extragastric diseases: a review. *World J Gastroenterol* 2018;24:3204–21.
13 Zuo Y, Jing Z, Bie M, *et al*. Association between helicobacter pylori infection and the risk of colorectal cancer: a systematic review and meta-analysis. *Medicine (Baltimore)* 2020;99:e21832.
14 Ralser A, Mejias-Luque R, Gerhard M. *Data from: helicobacter pylori in colorectal carcinogenesis*. NCBI BioProject, 2023. Available: https://www.ncbi.nlm.nih.gov/bioproject/PRJNA808836/
15 Becht E, McInnes L, Healy J, *et al*. Dimensionality reduction for visualizing single-cell data using UMAP. *Nat Biotechnol* 3, 2018.
16 Osman A, Yan B, Li Y, *et al*. Tcf-1 controls Treg cell functions that regulate inflammation, CD8+ T cell cytotoxicity and severity of colon cancer. *Nat Immunol* 2021;22:1152–62.
17 Miragaia RJ, Gomes T, Chomka A, *et al*. Single-cell transcriptomics of regulatory T cells reveals trajectories of tissue adaptation. *Immunity* 2019;50:493–504.
18 Vasanthakumar A, Liao Y, Teh P, *et al*. The TNF receptor superfamily-NF-κb axis is critical to maintain effector regulatory T cells in lymphoid and non-lymphoid tissues. *Cell Rep* 2017;20:2906–20.
19 La Manno G, Soldatov R, Zeisel A, *et al*. Rna velocity of single cells. *Nature* 2018;560:494–8.
20 Parikh K, Antanaviciute A, Fawkner-Corbett D, *et al*. Colonic epithelial cell diversity in health and inflammatory bowel disease. *Nature* 2019;567:49–55.
21 Moor AE, Harnik Y, Ben-Moshe S, *et al*. Spatial reconstruction of single enterocytes uncovers broad zonation along the intestinal villus axis. *Cell* 2018;175:1156–67.
22 Brandt S, Kwok T, Hartig R, *et al*. Nf-Kappab activation and potentiation of proinflammatory responses by the Helicobacter pylori CagA protein. *Proc Natl Acad Sci U S A* 2005;102:9300–5.
23 Menheniott TR, Judd LM, Giraud AS. Stat3: a critical component in the response to Helicobacter pylori infection. *Cell Microbiol* 2015;17:1570–82.
24 Bollrath J, Phesse TJ, von Burstin VA, *et al*. Gp130-Mediated STAT3 activation in enterocytes regulates cell survival and cell-cycle progression during colitis-associated tumorigenesis. *Cancer Cell* 2009;15:91–102.
25 Nguyen AV, Wu Y-Y, Liu Q, *et al*. Stat3 in epithelial cells regulates inflammation and tumor progression to malignant state in colon. *Neoplasia* 2013;15:998–1008.
26 Asada R, Saito A, Kawasaki N, *et al*. The endoplasmic reticulum stress transducer OASIS is involved in the terminal differentiation of goblet cells in the large intestine. *J Biol Chem* 2012;287:8144–53.
27 Aden K, Rehman A, Falk-Paulsen M, *et al*. Epithelial IL-23R signaling licenses protective IL-22 responses in intestinal inflammation. *Cell Rep* 2016;16:2208–18.
28 Katoh M, Katoh M. Notch signaling in gastrointestinal tract (review). *Int J Oncol* 2007;30:247–51.
29 Wirbel J, Pyl PT, Kartal E, *et al*. Meta-Analysis of fecal metagenomes reveals global microbial signatures that are specific for colorectal cancer. *Nat Med* 2019;25:679–89.
30 Guo Y, Zhang Y, Gerhard M, *et al*. Effect of Helicobacter pylori on gastrointestinal microbiota: a population-based study in linqu, a high-risk area of gastric cancer. *Gut* 2020;69:1598–607.
31 Ohnmacht C, Park J-H, Cording S, *et al*. MUCOSAL IMMUNOLOGY. the microbiota regulates type 2 immunity through rorγT. *Science* 2015;349:989–93.
32 van Zanten SJOV, Kolesnikow T, Leung V, *et al*. Gastric transitional zones, areas where Helicobacter treatment fails: results of a treatment trial using the Sydney strain mouse model. *Antimicrob Agents Chemother* 2003;47:2249–55.
33 Franceschi F, Covino M, Roubaud Baudron C. Review: Helicobacter pylori and extragastric diseases. *Helicobacter* 2019;24 Suppl 1:e12636.
34 Kim TJ, Kim ER, Chang DK, *et al*. Helicobacter pylori infection is an independent risk factor of early and advanced colorectal neoplasm. *Helicobacter* 2017;22.
35 Arnold IC, Dehzad N, Reuter S, *et al*. Helicobacter pylori infection prevents allergic asthma in mouse models through the induction of regulatory T cells. *J Clin Invest* 2011;121:3088–93.
36 Caruso R, Fina D, Paoluzi OA, *et al*. IL-23-mediated regulation of IL-17 production in Helicobacter pylori-infected gastric mucosa. *Eur J Immunol* 2008;38:470–8.
37 Tosolini M, Kirilovsky A, Mlecnik B, *et al*. Clinical impact of different classes of infiltrating T cytotoxic and helper cells (Th1, Th2, Treg, Th17) in patients with colorectal cancer. *Cancer Res* 2011;71:1263–71.
38 Du R, Zhao H, Yan F, *et al*. IL-17+foxp3+ T cells: an intermediate differentiation stage between Th17 cells and regulatory T cells. *J Leukoc Biol* 2014;96:39–48.
39 Ma C, Dong X. Colorectal cancer-derived FOXP3 (+) IL-17 (+) T cells suppress tumour-specific CD8+ T cells. *Scand J Immunol* 2011;74:47–51.

40 Yang S, Wang B, Guan C, *et al*. Foxp3+IL-17+ T cells promote development of cancer-initiating cells in colorectal cancer. *J Leukoc Biol* 2011;89:85–91.
41 Sinicrope FA, Rego RL, Ansell SM, *et al*. Intraepithelial effector (CD3+) /regulatory (Foxp3+) T-cell ratio predicts a clinical outcome of human colon carcinoma. *Gastroenterology* 2009;137:1270–9.
42 Smith G, Carey FA, Beattie J, *et al*. Mutations in APC, Kirsten-ras, and p53 -- alternative genetic pathways to colorectal cancer. *Proc Natl Acad Sci U S A* 2002;99:9433–8.
43 Janssen K-P, Alberici P, Fsihi H, *et al*. Apc and oncogenic KRAS are synergistic in enhancing Wnt signaling in intestinal tumor formation and progression. *Gastroenterology* 2006;131:1096–109.
44 Schwitalla S, Fingerle AA, Cammareri P, *et al*. Intestinal tumorigenesis initiated by dedifferentiation and acquisition of stem-cell-like properties. *Cell* 2013;152:25–38.
45 Eaden JA, Abrams KR, Mayberry JF. The risk of colorectal cancer in ulcerative colitis: a meta-analysis. *Gut* 2001;48:526–35.
46 Waldner MJ, Neurath MF. Mechanisms of immune signaling in colitis-associated cancer. *Cell Mol Gastroenterol Hepatol* 2015;1:6–16.
47 Kusaba T, Nakayama T, Yamazumi K, *et al*. Activation of STAT3 is a marker of poor prognosis in human colorectal cancer. *Oncol Rep* 2006;15:1445–51.
48 Musteanu M, Blaas L, Mair M, *et al*. Stat3 is a negative regulator of intestinal tumor progression in Apc (min) mice. *Gastroenterology* 2010;138:1003–11.
49 Chen Y, Vandereyken M, Newton IP, *et al*. Loss of adenomatous polyposis coli function renders intestinal epithelial cells resistant to the cytokine IL-22. *PLoS Biol* 2019;17:e3000540.
50 Li Y, Kundu P, Seow SW, *et al*. Gut microbiota accelerate tumor growth via c-Jun and STAT3 phosphorylation in ApcMin/+ mice. *Carcinogenesis* 2012;33:1231–8.
51 Compare D, Nardone G. Contribution of gut microbiota to colonic and extracolonic cancer development. *Dig Dis* 2011;29:554–61.
52 Wick EC, Rabizadeh S, Albesiano E, *et al*. Stat3 activation in murine colitis induced by enterotoxigenic Bacteroides fragilis. *Inflamm Bowel Dis* 2014;20:821–34.
53 Iino C, Shimoyama T. Impact of Helicobacter pylori infection on gut microbiota. *World J Gastroenterol* 2021;27:6224–30.
54 Kienesberger S, Cox LM, Livanos A, *et al*. Gastric helicobacter pylori infection affects local and distant microbial populations and host responses. *Cell Rep* 2016;14:1395–407.
55 Uronis JM, Mühlbauer M, Herfarth HH, *et al*. Modulation of the intestinal microbiota alters colitis-associated colorectal cancer susceptibility. *PLoS One* 2009;4:e6026.
56 Wang L, Tang L, Feng Y, *et al*. A purified membrane protein from akkermansia muciniphila or the pasteurised bacterium blunts colitis associated tumourigenesis by modulation of CD8+ T cells in mice. *Gut* 2020;69:1988–97.
57 Weir TL, Manter DK, Sheflin AM, *et al*. Stool microbiome and metabolome differences between colorectal cancer patients and healthy adults. *PLoS One* 2013;8:e70803.

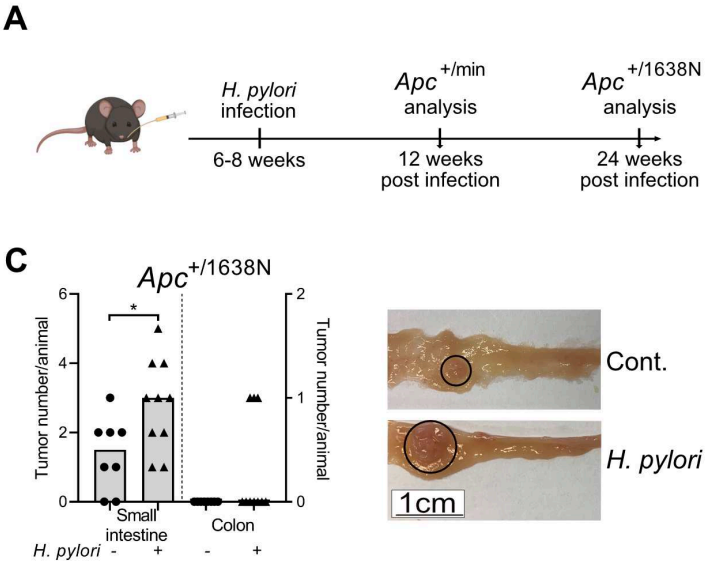
A
H. pylori infection
6-8 weeks
Apc+/min analysis
12 weeks post infection
Apc+/1638N analysis
24 weeks post infection
B
Apc+/min
Apc+/1638N
CFU/mg stomach (log10)
Stomach
Small intestine
Colon
C
Apc+/1638N
Tumor number/animal
Small intestine
Colon
H. pylori
Cont.
H. pylori
1cm

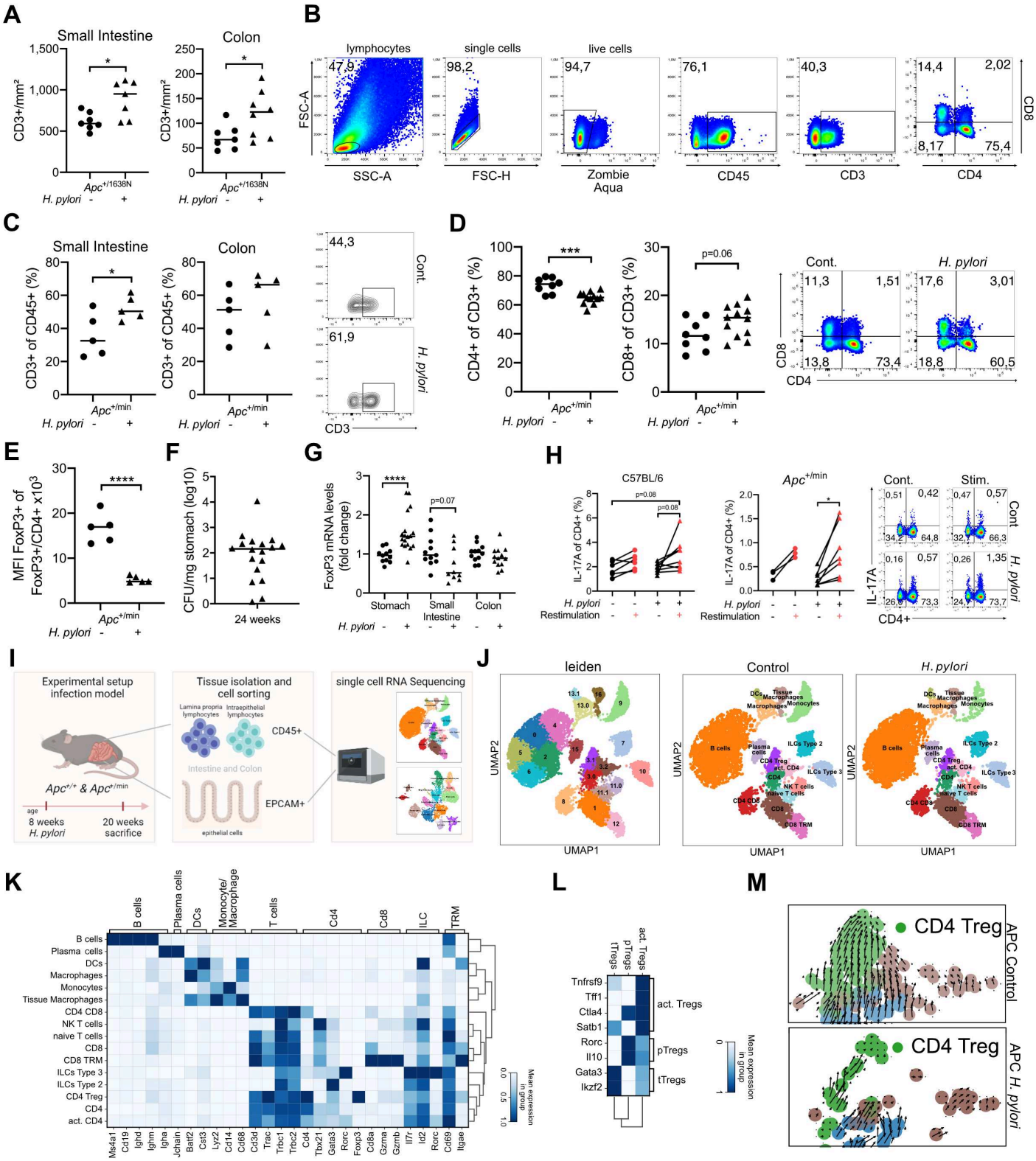
A
Small Intestine
Colon
CD3+/mm²
Apc+/1638N
H. pylori
B
lymphocytes
single cells
live cells
FSC-A
SSC-A
FSC-H
Zombie Aqua
CD45
CD3
CD4
CD8
C
CD3+ of CD45+ (%)
Apc+/min
Cont.
H. pylori
CD3
D
CD4+ of CD3+ (%)
CD8+ of CD3+ (%)
p=0.06
CD8
CD4
E
MFI FoxP3+ of FoxP3+/CD4+ x10³
F
CFU/mg stomach (log10)
24 weeks
G
FoxP3 mRNA levels (fold change)
p=0.07
Stomach
Small Intestine
Colon
H
C57BL/6
Apc+/min
IL-17A of CD4+ (%)
Restimulation
Stim.
IL-17A
CD4+
I
Experimental setup infection model
Apc+/+ & Apc+/min
age
8 weeks
H. pylori
20 weeks
sacrifice
Tissue isolation and cell sorting
Lamina propria lymphocytes
Intraepithelial lymphocytes
CD45+
Intestine and Colon
EPCAM+
epithelial cells
single cell RNA Sequencing
J
leiden
Control
H. pylori
UMAP1
UMAP2
B cells
Plasma cells
DCs
Tissue Macrophages
Macrophages
Monocytes
ILCs Type 2
CD4 Treg
act. CD4
ILCs Type 3
CD4
NK T cells
naive T cells
CD4 CD8
CD8
CD8 TRM
K
B cells
Plasma cells
DCs
Monocyte/ Macrophage
T cells
Cd4
Cd8
ILC
TRM
Macrophages
Monocytes
Tissue Macrophages
CD4 CD8
NK T cells
naive T cells
CD8
CD8 TRM
ILCs Type 3
ILCs Type 2
CD4 Treg
CD4
act. CD4
Ms4a1
Cd19
Ighd
Ighm
Igha
Jchain
Batf2
Csf3
Lyz2
Cd14
Cd68
Cd3d
Trac
Trbc1
Trbc2
Cd4
Tbx21
Gata3
Rorc
Foxp3
Cd8a
Gzma
Gzmb
Il7r
Id2
Rorc
Cd69
Itgae
Mean expression in group
L
tTregs
pTregs
act. Tregs
Tnfrsf9
Tff1
Ctla4
Satb1
Rorc
Il10
Gata3
Ikzf2
Mean expression in group
M
CD4 Treg
APC Control
APC H. pylori

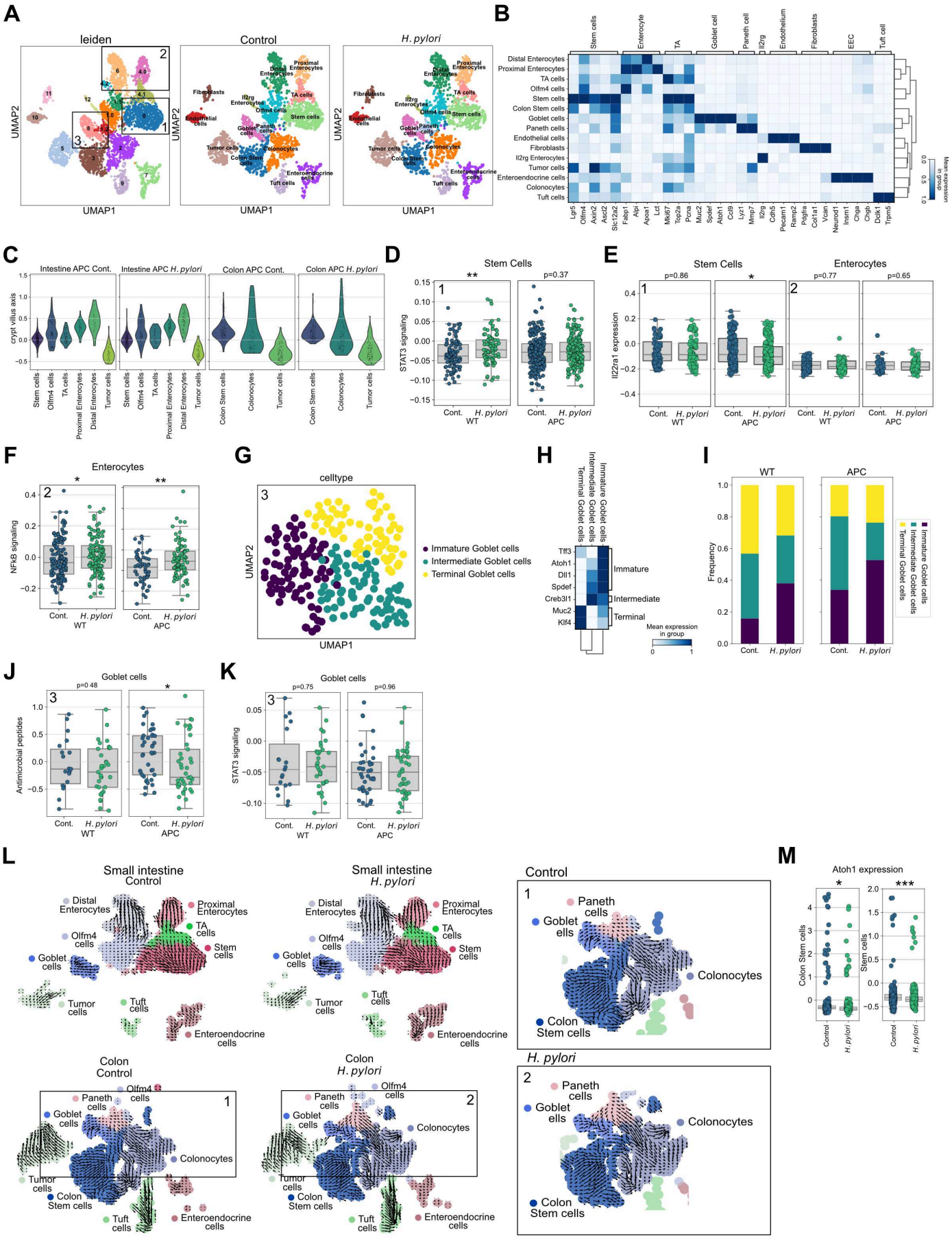
A
leiden
Control
H. pylori
UMAP1
UMAP2
B
Stem cells
Enterocyte
TA
Goblet cell
Paneth cell
Il2rg
Endothelium
Fibroblasts
EEC
Tuft cell
Distal Enterocytes
Proximal Enterocytes
TA cells
Olfm4 cells
Stem cells
Colon Stem cells
Goblet cells
Paneth cells
Endothelial cells
Fibroblasts
Il2rg Enterocytes
Tumor cells
Enteroendocrine cells
Colonocytes
Tuft cells
C
Intestine APC Cont.
Intestine APC H. pylori
Colon APC Cont.
Colon APC H. pylori
crypt villus axis
D
Stem Cells
STAT3 signaling
E
Stem Cells
Enterocytes
Il22ra1 expression
F
Enterocytes
NFκB signaling
G
celltype
Immature Goblet cells
Intermediate Goblet cells
Terminal Goblet cells
H
Tff3
Atoh1
Dll1
Spdef
Creb3l1
Muc2
Klf4
Immature
Intermediate
Terminal
Mean expression in group
I
WT
APC
Frequency
J
Goblet cells
Antimicrobial peptides
p=0.48
K
Goblet cells
STAT3 signaling
p=0.75
p=0.96
L
Small intestine Control
Small intestine H. pylori
Colon Control
Colon H. pylori
Control
H. pylori
M
Atoh1 expression
Colon Stem cells
Stem cells
Cont.
H. pylori
WT
APC

Treg_effector_score

Genes	Source
Tnfrsf4	PMID: 28889989
Tnfrsf8	
Tnfrsf9	
Tnfrsf14	
Tnfrsf18	
Tnfrsf10	
Tnfrsf1b	

Th17_differentiation

Genes	Source
Tgfb1	PMID: 34385712
Il6ra	
Rara	
Stat3	
Ifngr2	
Gata3	
Tbx21	

crypt_villus_axis

Genes	Source
Plac8	PMID: 30814735, 30270040
Ceacam1	
Tspan1	
Ifi27	
Dhrs9	
Krt20	
Rhoc	
Cd177	
Pkib	
Hpgd	
Lypd8	

STAT3_signaling

Genes	Genes	Genes	Genes
Akt2	*Ifne*	*Il5*	*Sos2*
Akt3	*Ifng*	*Il5ra*	*Spred1*
Bcl2l1	*Ifngr1*	*Il6*	*Spred2*
Cbl	*Ifngr2*	*Il6r*	*Spry1*
Cblb	*Ifnk*	*Il6st*	*Spry2*
Cblc	*Ifnl1*	*Il7*	*Spry3*
Ccnd1	*Ifnl2*	*Il7r*	*Spry4*
Ccnd2	*Ifnl3*	*Il9*	*Stam*
Ccnd3	*Ifnlr1*	*Il9r*	*Stam2*
Cish	*Ifnw1*	*Irf9*	*Stat1*
Clcf1	*Il10*	*Jak1*	*Stat2*
Cntf	*Il10ra*	*Jak2*	*Stat3*
Cntfr	*Il10rb*	*Jak3*	*Stat4*
Crebbp	*Il11*	*Lep*	*Stat5a*
Crlf2	*Il11ra*	*Lepr*	*Stat5b*
Csf2	*Il12a*	*Lif*	*Stat6*
Csf2ra	*Il12b*	*Lifr*	*Tpo*
Csf2rb	*Il12rb1*	*Mpl*	*Tslp*
Csf3	*Il12rb2*	*Myc*	*Tyk2*
Csf3r	*Il13*	*Osm*	
Csh1	*Il13ra1*	*Osmr*	
Ctf1	*Il13ra2*	*Pias1*	
Ep300	*Il15*	*Pias2*	
Epo	*Il15ra*	*Pias3*	
Epor	*Il19*	*Pias4*	
Gh1	*Il2*	*Pik3ca*	
Gh2	*Il20*	*Pik3cb*	
Ghr	*Il20ra*	*Pik3cd*	
Grb2	*Il20rb*	*Pik3cg*	
Ifna1	*Il21*	*Pik3r1*	
Ifna10	*Il21r*	*Pik3r2*	
Ifna13	*Il22*	*Pik3r3*	
Ifna14	*Il22ra1*	*Pik3r5*	
Ifna16	*Il22ra2*	*Pim1*	
Ifna17	*Il23a*	*Prl*	
Ifna2	*Il23r*	*Prlr*	
Ifna21	*Il24*	*Ptpn11*	
Ifna4	*Il26*	*Ptpn6*	
Ifna5	*Il2ra*	*Socs1*	
Ifna6	*Il2rb*	*Socs2*	
Ifna7	*Il2rg*	*Socs3*	
Ifna8	*Il3*	*Socs4*	
Ifnar1	*Il3ra*	*Socs5*	
Ifnar2	*Il4*	*Socs7*	
Ifnb1	*Il4r*	*Sos1*	

Source
KEGG, GSEA.
PMID: 10592173, 16199517

NFkB_signaling

Genes
Fadd
Ikbkb
Ikbkg
Il1a
Il1r1
Map3k1
Map3k14
Map3k7
Myd88
Nfkb1
Nfkbia
Rela
Ripk1
Tab1
Tnf
Tnfaip3
Tnfrsf1a
Tnfrsf1b
Tradd
Traf6

Source
KEGG, GSEA.
PMID: 10592173, 16199517

Antimicrobial_peptides

Genes
Reg3b
Reg3a
Reg3g

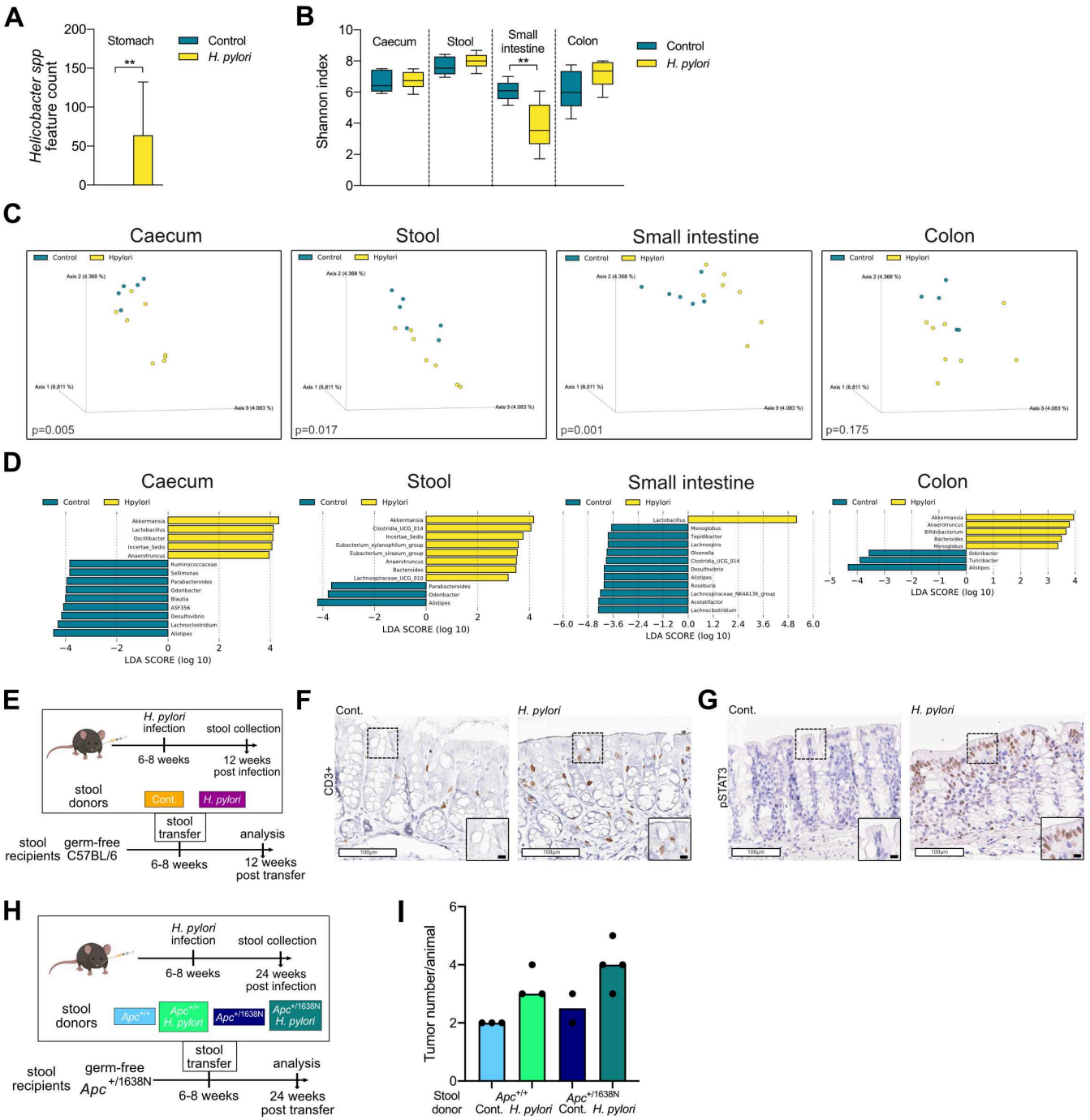
A
Stomach
Control
H. pylori
Helicobacter spp feature count
**
B
Caecum
Stool
Small intestine
Colon
Shannon index
Control
H. pylori
**
C
Caecum
Stool
Small intestine
Colon
Control
Hpylori
p=0.005
p=0.017
p=0.001
p=0.175
D
Caecum
Stool
Small intestine
Colon
LDA SCORE (log 10)
E
H. pylori infection
stool collection
6-8 weeks
12 weeks post infection
stool donors
Cont.
H. pylori
stool recipients
germ-free C57BL/6
stool transfer
analysis
6-8 weeks
12 weeks post transfer
F
Cont.
H. pylori
CD3+
G
Cont.
H. pylori
pSTAT3
H
H. pylori infection
stool collection
6-8 weeks
24 weeks post infection
stool donors
Apc+/+
Apc+/+ H. pylori
Apc+/1638N
Apc+/1638N H. pylori
stool recipients
germ-free Apc+/1638N
stool transfer
analysis
6-8 weeks
24 weeks post transfer
I
Tumor number/animal
Stool donor
Apc+/+ Cont.
Apc+/+ H. pylori
Apc+/1638N Cont.
Apc+/1638N H. pylori

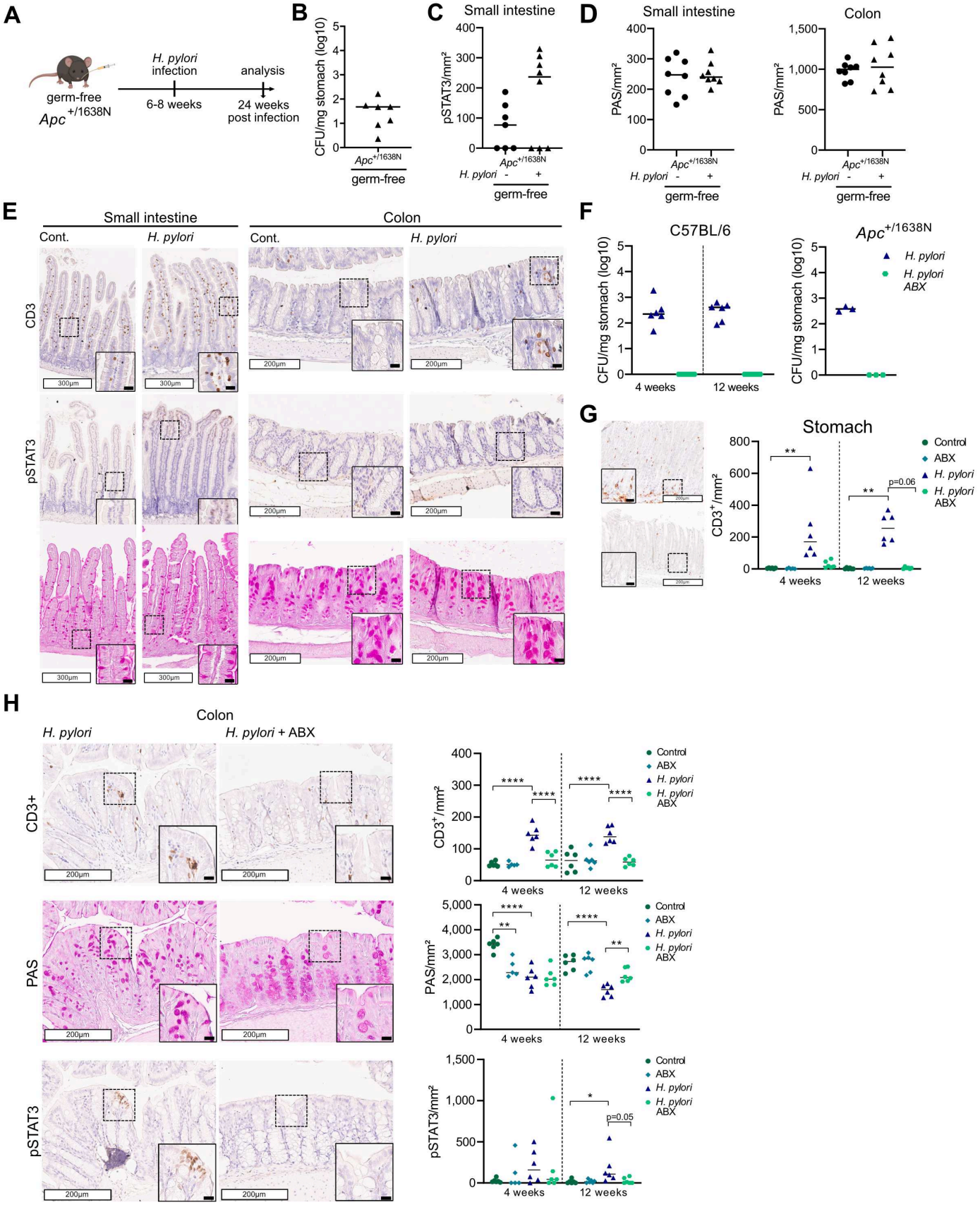
A
germ-free
Apc+/1638N
H. pylori infection
6-8 weeks
analysis
24 weeks post infection
B
CFU/mg stomach (log10)
Apc+/1638N
germ-free
C
Small intestine
pSTAT3/mm²
H. pylori
D
Small intestine
Colon
PAS/mm²
E
Small intestine
Colon
Cont.
H. pylori
CD3
pSTAT3
300µm
200µm
F
C57BL/6
Apc+/1638N
CFU/mg stomach (log10)
4 weeks
12 weeks
H. pylori
H. pylori ABX
G
Stomach
CD3+/mm²
Control
ABX
H. pylori
H. pylori ABX
p=0.06
H
Colon
H. pylori
H. pylori + ABX
CD3+
PAS
pSTAT3
p=0.05

ID	Sex	Age group	*H. pylori*	Type	Gastrointestinal disease
1	m	75-79	negative	FFPE	no
2	m	65-69	negative	FFPE	no
3	f	65-69	negative	FFPE	Vit B12 anaemia
4	f	50-54	negative	FFPE	no
5	m	30-34	negative	FFPE	no
6	m	15-19	negative	FFPE	Crohn's disease
7	m	10-14	negative	FFPE	small duodenal erosion
8	f	65-69	negative	FFPE	no
9	m	10-19	negative	FFPE	Crohn's disease
10	m	30-34	negative	FFPE	Crohn's disease
11	f	50-54	negative	FFPE	no
12	f	50-54	negative	FFPE	no
13	f	50-54	negative	FFPE	no
14	f	25-29	negative	FFPE	no
15	m	30-34	negative	FFPE	no
16	f	30-34	negative	FFPE	no
17	m	45-49	negative	FFPE	no
18	m	75-79	negative	FFPE	Rectum carcinoma
19	f	30-34	negative	FFPE	no
20	f	20-24	negative	FFPE	no
21	m	30-34	negative	FFPE	no
22	m	80-84	negative	FFPE	Sigma carcinoma 2006
23	f	35-39	negative	FFPE	no
24	f	50-54	negative	FFPE	Collagenous colitis
25	f	5-9	negative	FFPE	no
26	f	80-84	negative	FFPE	no
27	m	65-69	negative	FFPE	no
28	f	55-59	negative	FFPE	no
29	f	65-69	negative	FFPE	no
30	m	65-69	negative	FFPE	no
31	f	60-64	negative	FFPE	no
32	m	35-39	negative	FFPE	Barrett
33	f	25-29	negative	FFPE	no
34	m	35-39	negative	FFPE	no
35	f	70-74	negative	FFPE	no
36	m	20-24	negative	FFPE	no
37	f	60-64	negative	FFPE	no
38	m	60-64	negative	FFPE	no
39	m	45-49	negative	FFPE	Crohn's disease
40	m	75-79	negative	FFPE	Colon adenomas, Barrett
41	f	80-84	negative	FFPE	Colon adenomas
42	f	50-54	negative	FFPE	no
43	f	25-29	negative	FFPE	no
44	f	60-64	negative	FFPE	no

ID	Sex	Age group	*H. pylori*	Type	Gastrointestinal disease
45	m	75-79	negative	FFPE	Colon adenomas
46	m	75-79	negative	FFPE	Colon adenomas
47	f	50-54	negative	FFPE	no
48	f	80-84	positive	FFPE	Ulcer
49	m	55-59	positive	FFPE	no
50	f	70-74	positive	FFPE	no
51	f	25-29	positive	FFPE	no
52	f	55-59	positive	FFPE	Infectious colitis
53	m	65-69	positive	FFPE	HGD in Sigmoid
54	m	35-39	positive	FFPE	Crohn's disease
55	m	60-64	positive	FFPE	no
56	f	50-54	positive	FFPE	Crohn's disease
57	f	70-74	positive	FFPE	no
58	f	70-74	positive	FFPE	Malt lymphoma rectum
59	m	50-54	positive	FFPE	no
60	m	55-59	positive	FFPE	no
61	m	75-79	positive	FFPE	Colon adenomas
62	m	45-49	positive	FFPE	no
63	m	70-74	positive	FFPE	Colon adenomas
64	f	30-34	positive	FFPE	no
65	f	20-24	positive	FFPE	no
66	m	35-39	positive	FFPE	CMV colitis
67	f	60-64	positive	FFPE	Cajal cell hypoplasia
68	m	50-54	negative	Endoscopic Biopsy	Carcinoma undifferentiated
69	m	75-79	negative	Endoscopic Biopsy	no
70	m	70-74	negative	Endoscopic Biopsy	no
71	m	80-84	negative	Endoscopic Biopsy	no
72	m	70-74	negative	Endoscopic Biopsy	no
73	f	55-59	negative	Endoscopic Biopsy	no
74	f	60-64	negative	Endoscopic Biopsy	no
75	f	70-74	negative	Endoscopic Biopsy	no
76	f	75-79	negative	Endoscopic Biopsy	no
77	f	70-74	negative	Endoscopic Biopsy	no
78	f	25-29	negative	Endoscopic Biopsy	no
79	f	70-74	negative	Endoscopic Biopsy	no
80	f	75-79	negative	Endoscopic Biopsy	no
81	m	75-79	negative	Endoscopic Biopsy	no
82	f	60-64	negative	Endoscopic Biopsy	no
83	m	55-59	negative	Endoscopic Biopsy	no
84	m	75-79	negative	Endoscopic Biopsy	no
85	f	75-79	negative	Endoscopic Biopsy	no
86	f	70-74	negative	Endoscopic Biopsy	no
87	m	20-24	negative	Endoscopic Biopsy	no
88	f	40-44	negative	Endoscopic Biopsy	no

ID	Sex	Age group	*H. pylori*	Type	Gastrointestinal disease
89	m	45-49	negative	Endoscopic Biopsy	no
90	m	20-24	negative	Endoscopic Biopsy	no
91	f	75-79	negative	Endoscopic Biopsy	no
92	f	70-74	negative	Endoscopic Biopsy	no
93	f	55-59	negative	Endoscopic Biopsy	Crohn's disease
94	f	80-84	negative	Endoscopic Biopsy	no
95	m	50-54	negative	Endoscopic Biopsy	no
96	m	55-59	negative	Endoscopic Biopsy	no
97	f	40-44	negative	Endoscopic Biopsy	no
98	m	30-34	negative	Endoscopic Biopsy	no
99	f	65-69	negative	Endoscopic Biopsy	no
100	m	80-84	negative	Endoscopic Biopsy	no
101	m	50-54	negative	Endoscopic Biopsy	no
102	m	65-69	negative	Endoscopic Biopsy	no
103	m	75-79	negative	Endoscopic Biopsy	no
104	m	55-59	negative	Endoscopic Biopsy	no
105	f	20-24	negative	Endoscopic Biopsy	no
106	m	40-44	negative	Endoscopic Biopsy	no
107	m	65-69	negative	Endoscopic Biopsy	no
108	f	35-39	negative	Endoscopic Biopsy	no
109	f	35-39	negative	Endoscopic Biopsy	no
110	f	60-64	negative	Endoscopic Biopsy	no
111	f	25-29	negative	Endoscopic Biopsy	no
112	f	25-29	negative	Endoscopic Biopsy	no
113	m	50-54	negative	Endoscopic Biopsy	no
114	m	55-59	negative	Endoscopic Biopsy	no
115	m	40-44	negative	Endoscopic Biopsy	Ulcerative colitis
116	f	40-44	negative	Endoscopic Biopsy	no
117	f	60-64	negative	Endoscopic Biopsy	no
118	m	75-79	negative	Endoscopic Biopsy	no
119	m	65-69	negative	Endoscopic Biopsy	no
120	f	30-34	negative	Endoscopic Biopsy	no
121	f	70-74	negative	Endoscopic Biopsy	no
122	f	40-44	negative	Endoscopic Biopsy	Crohn's disease
123	m	25-29	negative	Endoscopic Biopsy	no
124	m	70-74	negative	Endoscopic Biopsy	no
125	m	70-74	negative	Endoscopic Biopsy	no
126	f	30-34	negative	Endoscopic Biopsy	Ulcerative colitis
127	m	60-64	negative	Endoscopic Biopsy	no
128	f	55-59	negative	Endoscopic Biopsy	no
129	f	25-29	negative	Endoscopic Biopsy	no
130	m	55-59	negative	Endoscopic Biopsy	no
131	f	60-64	positive	Endoscopic Biopsy	no
132	f	50-54	positive	Endoscopic Biopsy	no

ID	Sex	Age group	*H. pylori*	Type	Gastrointestinal disease
133	f	60-64	positive	Endoscopic Biopsy	no
134	f	75-79	positive	Endoscopic Biopsy	Crohn's disease
135	m	40-44	positive	Endoscopic Biopsy	no
136	f	75-79	positive	Endoscopic Biopsy	no
137	m	65-69	positive	Endoscopic Biopsy	no
138	f	75-79	positive	Endoscopic Biopsy	no
139	m	55-59	positive	Endoscopic Biopsy	no
140	m	50-54	positive	Endoscopic Biopsy	Ulcerative colitis
141	f	55-59	positive	Endoscopic Biopsy	no
142	m	80-84	positive	Endoscopic Biopsy	no
143	m	60-64	positive	Endoscopic Biopsy	no
144	m	30-34	positive	Endoscopic Biopsy	no
145	f	40-44	positive	Endoscopic Biopsy	Crohn's disease
146	m	35-39	positive	Endoscopic Biopsy	no
147	m	70-74	positive	Endoscopic Biopsy	no
148	m	55-59	positive	Endoscopic Biopsy	no
149	m	55-59	positive	Endoscopic Biopsy	no
150	m	35-39	positive	Endoscopic Biopsy	Crohn's disease
151	m	65-69	positive	Endoscopic Biopsy	no
152	m	65-69	positive	Endoscopic Biopsy	no
153	f	65-69	positive	Endoscopic Biopsy	no
154	m	20-24	positive	Endoscopic Biopsy	no

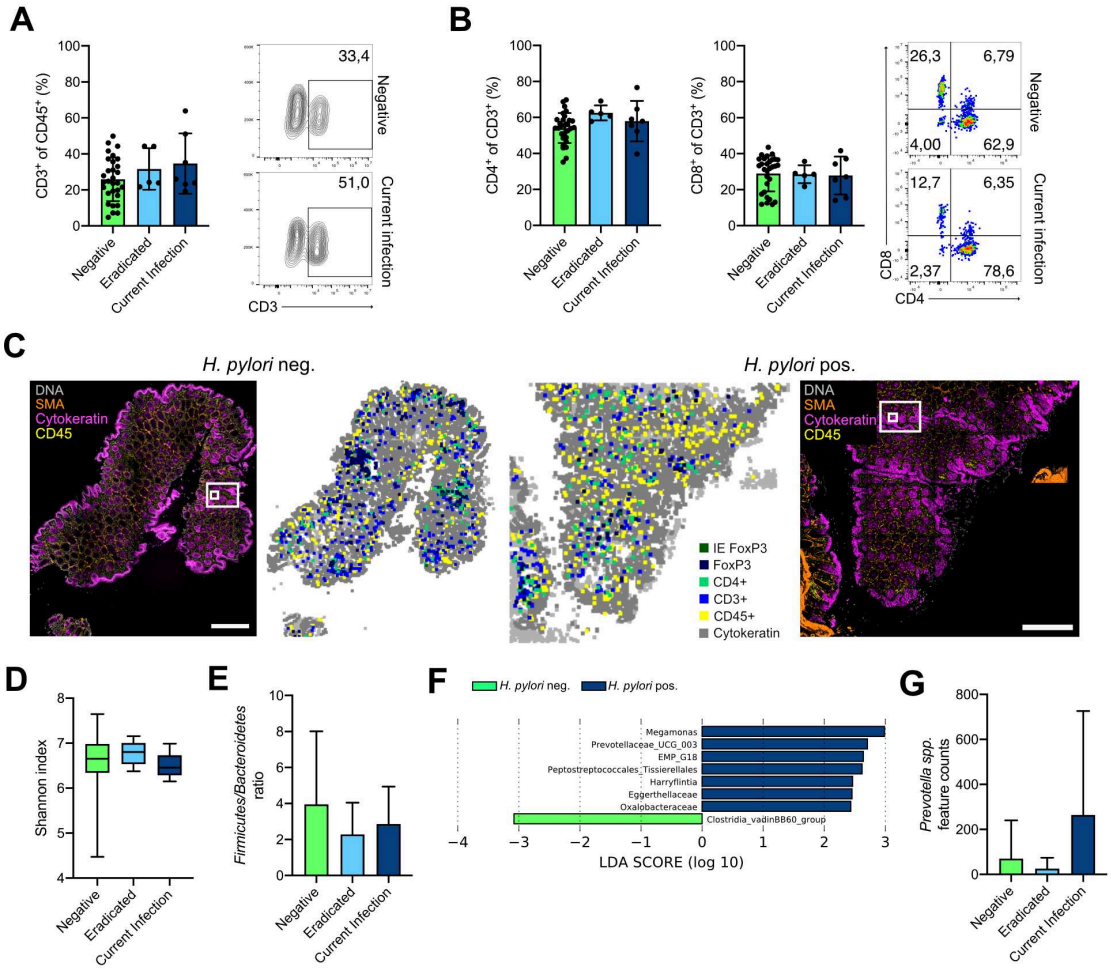
A
CD3+ of CD45+ (%)
Negative
Eradicated
Current Infection
33,4
51,0
CD3
B
CD4+ of CD3+ (%)
CD8+ of CD3+ (%)
26,3
6,79
4,00
62,9
12,7
6,35
2,37
78,6
CD8
CD4
C
H. pylori neg.
H. pylori pos.
DNA
SMA
Cytokeratin
CD45
IE FoxP3
FoxP3
CD4+
CD3+
CD45+
Cytokeratin
D
Shannon index
E
Firmicutes/Bacteroidetes ratio
F
H. pylori neg.
H. pylori pos.
Megamonas
Prevotellaceae_UCG_003
EMP_G18
Peptostreptococcales_Tissierellales
Harryflintia
Eggerthellaceae
Oxalobacteraceae
Clostridia_vadinBB60_group
LDA SCORE (log 10)
G
Prevotella spp. feature counts

MATERIALS AND METHODS

STUDY DESIGN

This study was conceptualized to investigate the underlying mechanisms of *H. pylori* induced colorectal carcinogenesis.

Tumor mouse models *Apc*$^{+/min}$, initially obtained from Jackson Laboratories, and *Apc*$^{+/1638N}$ mice, provided by Prof. Klaus-Peter Janssen (Klinikum rechts der Isar, München) (1), were bred under specific pathogen-free conditions at our animal facility at the Technical University of Munich. Both female and male mice were used and co-housed with littermate controls.

C57BL/6 mice, *Apc*$^{+/1638N}$ mice and wild type littermates were re-derived germ-free from conventional mice by Prof. Bleich and Dr. Basic (Hannover medical school, Hannover).

Female C57BL/6 mice were purchased from Envigo RMS GmbH at an age of 6 weeks and acclimatized to our animal facility for 1-2 weeks prior infection. Mice were fed with a standard diet and water ad libitum and maintained under a 12-hour light-dark cycle. DNA extracted from mouse tails was used for genotyping. All animal experiments were conducted in compliance with European guidelines for the care and use of laboratory animals and were approved by the Bavarian Government (Regierung von Oberbayern, Az.55.2-1-54-2532-161-2017).

87 fresh colonoscopy biopsies were collected within the framework of the ColoBAC study of the CRC1371 (Dept. of Surgery and II. Medical Dept. Klinikum rechts der Isar, Technical University of Munich, Germany). 67 FFPE colon biopsies were obtained from the Klinikum Bayreuth. Both studies were approved by the respective ethics committees (Klinikum rechts der Isar #322/18, Klinikum Bayreuth #241_20Bc).

H. pylori status of colonoscopy biopsies was determined in serum samples using the recomwell Helicobacter IgG kit (Mikrogen) according to manufacturer's instructions. *H. pylori* status of FFPE biopsies was determined histologically in corresponding gastric biopsies by Prof. Michael Vieth (Table S2).

H. PYLORI INFECTION

H. pylori pre-mouse Sidney Strain 1 (PMSS1) was cultured on Wilkins-Chalgren (WC) Dent (containing vancomycin, trimethoprim, cefsoludin and amphotericin) agar plates in a microaerophilic atmosphere (5% O2, 10% CO2). 6–8-week old mice were orally gavaged twice within 72 hours with 2 × 10^8 *H. pylori* PMSS1 in 200 µl brain-heart-infusion (BHI) medium containing 20% fetal calve serum (FCS). Infection status was determined by plating homogenized stomach, intestinal and colonic tissue on WC Dent plates supplemented with 200 g/ml bacitracin, 10 g/ml nalidixic acid and 3 g/ml polymycin B, and counting colony-forming units (CFU).

H. PYLORI ERADICATION

After 4 weeks of infection, *H. pylori* eradication was performed with an antibiotic cocktail containing clarithromycin (Eberth) (7.15 mg/kg/day), metronidazole (Carl Roth) (14.2 mg/kg/day) and the proton-pump inhibitor omeprazole (Carl Roth) (400 µmol/kg/day) by oral gavage twice daily for 7 consecutive days. Omeprazole was dissolved in 200µl 2.5% Hydroxy-propyl-methyl-cellulose (Sigma-Aldrich) with pH adjusted to 9. Antibiotics, dissolved in 200µl PBS, were administered 45 minutes after omeprazole (2).

STOOL TRANSFER

SPF *Apc*$^{+/1638N}$ mice and wild type littermates were infected at an age of 6-8 weeks and after 12 or 24 weeks of infection, stool pellets were collected from these “donor” mice, dissolved in 0.1ml PBS/g stool and administered via oral gavage to germ-free C57BL/6 or *Apc*$^{+/1638N}$ “recipient” mice.

HISTOLOGY AND IMMUNOHISTOCHEMISTRY

Small intestine and colon were longitudinally opened and flushed with phosphate-buffered saline (PBS). Solid neoplastic lesions were assessed and measured macroscopically by two independent examiners. Dissected tissue was fixed in 4% formaldehyde, embedded in paraffin and 4µm thick sections were used for staining. For immunohistochemical stainings, antigen retrieval was achieved with 10 mM sodium citrate (pH 6) or 1 mM EDTA (pH 8), and primary antibodies were applied overnight at 4°C (Table 1). Horseradish peroxidase (HRP) coupled secondary antibodies (Promega) and diaminobenzidine (DAB) (CellSignaling) were used to detect signal. Periodic acid Schiff (PAS) (Carl Roth) staining was performed to assess the quantity of mucus producing goblet cells. Stomach, intestinal and colonic sections were blindly quantified by two independent researchers by measuring the area of a functional unit (stomach gland, intestinal crypt/villus unit or colonic crypt) and counting positive cells per mm^2, using Aperio ImageScope (Leica BioSystems).

Table 1. Antibodies used for immunohistochemical evaluation.

Target	Clone	Origin/Target	Antigen retrieval	Dilution	Company
CD3	SP7	Rabbit mAB	sodium citrate	1:150	Thermo Fisher
Ki67	D3B5	Rabbit mAB	sodium citrate	1:400	Cell Signaling
pSTAT3	D3A7	Rabbit mAB	EDTA	1:200	Cell Signaling

CHIPCYTOMETRY AND AUTOMATIC IMAGE QUANTIFICATION

Murine intestinal and colonic cross-sections were preserved with O.C.T. compound (Tissue Tek) in cryomolds (Tissue Tek) and kept frozen at -80°C. For ChipCytometry, 7µm thick sections were cut on a Cryostat (Leica), fixed in Fixation Buffer (ZELLKRAFTWERK) for 45 minutes and subsequently transferred to CellSafe Chips (ZELLKRAFTWERK). ChipCytometry on human FFPE biopsies was performed according to the procedure described in Jarosch, Köhlen et al (3). Briefly, tissue sections were rehydrated on coverslips and antigen retrieval was performed using TRIS-EDTA buffer (pH 8.5) and then transferred to CellSafe Chips (ZELLKRAFTWERK). Alternating cycles of staining, immunofluorescence detection and photobleaching were performed for various markers (Table 2). Automated image processing was performed as described in Jarosch, Köhlen et al., which includes segmentation of cells, removing of outliers and spatial spill over correction (3). The resulting cell – marker matrix was analyzed using FlowJo software (V10.8.0), which enabled absolute quantification of cells.

Table 2. Antibodies used for ChipCytometry.

Epitope	Fluorochrome	Clone	Dilution	Company	Catalog #
anti-mouse CD3	PerCP/Cy5.5	17A2	1:200	BioLegend	100218
anti-mouse CD4	eFluor450	RM4-5	1:80	BioLegend	100531
anti-mouse CD45	FITC	30-F11	1:100	BioLegend	103108
anti-mouse Foxp3	PE	FJK-16s	1:80	eBioscience	14-5773-82
Pan-cytokeratin	AlexaFluor 488	C-11	1:100	BioLegend	628602
Hoechst	BUV395	-	1:50.000	ThermoScientific	H3570
α-SMA	eFluor570	1A4	1:750	eBioscience	41-9760-80
anti-human CD3	unconjugated	SP7	1:150	ThermoScientific	RM-9107-S1
anti-human CD4	AlexaFluor 488	polyclonal	1:50	R&D Systems	FAB8165G
anti-human CD45	PerCP/Cy5.5	HI30	1:80	BioLegend	304028
anti-human Foxp3	PE	236A/E7	1:30	eBioscience	563791
2nd anti-rabbit	PE	Polyclonal	1:300	BioLegend	406421

LAMINA PROPRIA AND INTRAEPITHELIAL LYMPHOCYTE ISOLATION AND FLOW CYTOMETRY

Harvested intestinal tissue was cut open longitudinally after removing Peyer's Patches and adjacent tissue. Subsequently, tissue was treated with 30mM EDTA, filtered supernatants were collected as intraepithelial lymphocytes and remaining tissue was digested with 0.5mg/mL collagenase from Clostridium histolyticum Type IV (Sigma Aldrich) and 10µg/mL DNase I (Applichem). Filtered and centrifuged lamina propria cell suspensions were density separated using a Percoll gradient (Thermo Fisher).

Fresh human biopsies were collected in Hank's Balanced Salt Solution w/o Mg^{2+}/Ca^{2+} (HBSS) and digested with 0.1% collagenase from Clostridium histolyticum Type IV (Sigma Aldrich) for 30 min. at 37°C. Digestion was stopped by adding 20 mL HBSS and centrifugation twice. Isolated lymphocytes were frozen in Dimethyl sulfoxide (Applichem) + 20 % FCS at -80° C. Single cell suspensions were blocked with anti-mouse CD16/CD32 or anti human TruStain FcX and live/dead staining performed with Zombie Aqua (BioLegend) in PBS. Surface antibodies (Table 3) were diluted according to titration experiments and cells stained for 30 min at 4° C. For transcription factors, Foxp3 Transcription Factor Staining Buffer Set (eBioscience) was used according to manufacturer's instructions. For stimulation with whole *H. pylori* lysate, cells were stimulated for 12 hours with 20µg/mL PMSS1 lysate at 37° C and protein transport inhibitor Golgi Plug (BD Biosciences) added 1:1000 after 7 hours for a total of 5 hours. Stimulated cells were stained with intracellular cytokine staining kit according manufacturer's instructions (BD Biosciences). Stained single cell suspensions were acquired on a CytoFlex S (Beckman Coulter) and analyzed using FlowJo software (V10.8.0).

Table 3. Antibodies used for flow cytometry.

Epitope	Fluorochrome	Clone	Dilution	Catalog #	Company
anti-mouse CD16/CD32	-	93	1:500	14-0161-86	eBioscience
anti-mouse CD45	AlexaFluor 700	30-F11	1:400	103128	BioLegend
anti-mouse CD3ε	FITC	500A2	1:200	152304	BioLegend
anit-mouse CD4	BV605	RM4-5	1:250	100548	BioLegend
anti-mouse CD4	eFluor450	RM4-5	1:250	48-0042-82	eBioscience
anti-mouse CD8a	APC-H7	53.6-7	1:250	560182	BD Biosciences
anti-mouse FoxP3	eFluor450	FJKL-16s	1:200	45-5773-82	eBioscience
anti-mouse RORyt	PE	B2D	1:100	12-6988-82	eBioscience
anti-mouse IL-17A	APC	eBio17B7	1:150	17-7177-81	eBioscience
anti-human CD45	AlexaFluor 700	2D1	1:50	368514	BioLegend
anti-human CD3	FITC	OKT3	1:300	317306	BioLegend
anti-human CD4	PB450	SK3	1:30	344620	BioLegend
anti-human CD8	APC-H7	SK1 (RUO)	1:150	560179	BD Biosciences
anti-human FoxP3	PerCP/Cy5.5	PCH101		35-4776-42	eBioscience
Human TruStain FcX	-	-	1:500	422302	BioLegend

SINGLE CELL RNA SEQUENCING

Intestinal and colonic tissue was harvested and cells were isolated as described in section "Lymphocyte isolation and Flow cytometry". Single cell suspensions were stained with anti-mouse CD45 PB450 (Clone: 30-F11, BioLegend, #103126), anti-mouse EPCAM APC (Clone: G8.8, BioLegend, #118214) and Propidium Iodide (PI). CD45+ PI- and EPCAM+ PI- cells were sorted.

For cell hashing TotalSeq-B anti-mouse Hashtags 1, 2 and 5 to 8 (M1/42; 30-F11, Biolegend, 155831, 155833, 155839, 155841, 155843, 155845) were used at a dilution of 1:50.

Single cell RNA Sequencing was performed with 10X Genomics, according to manufacturer's instructions (Chromium™ Single Cell 3' GEM v3 kit). Sorted cells were centrifuged and resuspended in mastermix and 37.8 µl of water, before 70 µl of the cell suspension was transferred to the chip. QC was performed with a high sensitivity DNA Kit (Agilent) on a Bioanalyzer 2100, and libraries were quantified with the Qubit dsDNA HS assay kit (life technologies).

Libraries were pooled according to their minimal required read counts (20.000 reads/cell for gene expression libraries). Illumina paired end sequencing was performed with 150 cycles on a NovaSeq 6000.

Annotation was performed using cellranger (V5.0.0, 10X genomics) against the murine reference genome GRCm38 (mm10-2020-A). All subsequent analysis was performed using SCANPY V1.6 (4). Preprocessing was performed following the guidelines of best practice in single-cell RNA-seq analysis (5) and involved less than 15% mitochondrial genes, regressing out cell cycle, mitochondrial genes and total counts. The data was normalized per cell count and logarithmized. Genes used for gene scores are listed in online supplemental table 1 and the scores were computed with the SCANPY build in function "sc.tl.score_genes".

RNA velocities were calculated using velocyto (6) and analyzed with scVelo (V 0.2.3) (7).

16S RRNA SEQUENCING

Bacterial DNA extraction and 16S rRNA sequencing was either performed as described previously (8, 9) by the Core Facility Microbiome of the ZIEL Institute for Food & Health (Technical University of Munich) or as follows: small intestine and colon tissue were homogenized with a Precellys® 24 homogeniser (Avantor). Phenol chloroform DNA isolation and ethanol precipitation were performed following modified protocols of P.J. Turnbaugh et al., 2009 and E. G. Zoetendal et al. 2006 (10, 11). Subsequently, the V3/V4 region of the *16S rRNA* gene was amplified and double indexed using barcoding primers modeled after Kozich *et al*. PCR fragments were purified using magnetic AMPure XP beads (Beckman Coulter, USA) according to manufacturer's instructions (12). The final pooled library was sequenced on an Illumina MiSeq with Reagent Kit v3 (Ilumina) for 600 cycles of paired-end reads.

Raw sequences were analyzed using the Qiime2 platform (v2021.4) (13). In detail, denoising, removing of chimeras and generation of Amplicon Sequence Variants (ASVs) was performed with dada2. Subsequently, a phylogenetic tree was generated and diversity measures were calculated. Chao1 index was used to determine community alpha diversity. Taxonomic

classification was performed with a qiime2 feature classifier trained on the SILVA132 99% OTUs, specifically targeting the V3 region. Linear discriminant analysis effect size (LEfSe) determining differentially abundant features was performed on the online interface at http://huttenhower.sph.harvard.edu/lefse/, developed by Segata et al. (14).

QUANTITATIVE PCR

Stomach, small intestine and colon tissue were homogenized with Precellys® 24 homogeniser (Avantor) and RNA isolation was performed with a Maxwell 48 RSC simply RNA Tissue Kit on a Maxwell RSC Instrument (Promega). cDNA was synthesized with Moloney Murine Leukemia Virus Reverse Transcriptase RNase H- Point Mutant (Promega). Gene expression was assessed with GoTaq qPCR Mastermix (Promega) on a CFX384 system (Bio-Rad). The quantitative PCR consisted of 40 cycles of amplification with 15 sec denaturation at 95 ˚C, 1 min annealing and amplification at 60 ˚C. According to the ΔΔCT method, CT values were normalized to *Gapdh* and to uninfected controls, in order to determine fold changes in gene expression. The sequences of primers used are summarized in Table 3.

Table 3. Primer sequences used for qPCR.

Gene	Forward sequence	Reverse sequence
Gapdh	GCCTTCTCCATGGTGGTGAA	GCACAGTCAAGGCCGAGAAT
Foxp3	AGGAGCCGCAAGCTAAAAGC	TGCCTTCGTGCCCACTGT

STATISTICAL ANALYSIS

Statistical analysis was conducted on biological replicates as stated in the figure legends. Depending on Gaussian distribution, statistical significance between two groups was determined with unpaired student's t-test or Mann-Whitney-U test and for analysis among more than two groups, ordinary one-way analysis of variance with Tukey's multiple-comparisons test or Kruskal-Wallis-test with Dunn's multiple-comparisons test. P values below 0.05 were considered significant. Exact p values are stated when relevant. Statistical analysis was carried out using Prism 8 (GraphPad Software).

1. Janssen KP, Alberici P, Fsihi H, Gaspar C, Breukel C, Franken P, et al. APC and oncogenic KRAS are synergistic in enhancing Wnt signaling in intestinal tumor formation and progression. Gastroenterology. 2006;131(4):1096-109.
2. van Zanten SJ, Kolesnikow T, Leung V, O'Rourke JL, Lee A. Gastric transitional zones, areas where Helicobacter treatment fails: results of a treatment trial using the Sydney strain mouse model. Antimicrob Agents Chemother. 2003;47(7):2249-55.
3. Jarosch S, Köhlen J, Sarker RSJ, Steiger K, Janssen KP, Christians A, et al. Multiplexed imaging and automated signal quantification in formalin-fixed paraffin-embedded tissues by ChipCytometry. Cell Reports Methods. 2021;1(7).
4. Wolf FA, Angerer P, Theis FJ. SCANPY: large-scale single-cell gene expression data analysis. Genome Biol. 2018;19(1):15.
5. Luecken MD, Theis FJ. Current best practices in single-cell RNA-seq analysis: a tutorial. Mol Syst Biol. 2019;15(6):e8746.
6. La Manno G, Soldatov R, Zeisel A, Braun E, Hochgerner H, Petukhov V, et al. RNA velocity of single cells. Nature. 2018;560(7719):494-8.
7. Bergen V, Lange M, Peidli S, Wolf FA, Theis FJ. Generalizing RNA velocity to transient cell states through dynamical modeling. Nat Biotechnol. 2020;38(12):1408-14.
8. Reitmeier S, Kiessling S, Neuhaus K, Haller D. Comparing Circadian Rhythmicity in the Human Gut Microbiome. STAR Protoc. 2020;1(3):100148.
9. Reitmeier S, Kiessling S, Clavel T, List M, Almeida EL, Ghosh TS, et al. Arrhythmic Gut Microbiome Signatures Predict Risk of Type 2 Diabetes. Cell Host Microbe. 2020;28(2):258-72 e6.
10. Zoetendal EG, Heilig HG, Klaassens ES, Booijink CC, Kleerebezem M, Smidt H, et al. Isolation of DNA from bacterial samples of the human gastrointestinal tract. Nat Protoc. 2006;1(2):870-3.
11. Turnbaugh PJ, Hamady M, Yatsunenko T, Cantarel BL, Duncan A, Ley RE, et al. A core gut microbiome in obese and lean twins. Nature. 2009;457(7228):480-4.
12. Kozich JJ, Westcott SL, Baxter NT, Highlander SK, Schloss PD. Development of a dual-index sequencing strategy and curation pipeline for analyzing amplicon sequence data on the MiSeq Illumina sequencing platform. Appl Environ Microbiol. 2013;79(17):5112-20.
13. Bolyen E, Rideout JR, Dillon MR, Bokulich NA, Abnet CC, Al-Ghalith GA, et al. Reproducible, interactive, scalable and extensible microbiome data science using QIIME 2. Nat Biotechnol. 2019;37(8):852-7.
14. Segata N, Izard J, Waldron L, Gevers D, Miropolsky L, Garrett WS, et al. Metagenomic biomarker discovery and explanation. Genome Biol. 2011;12(6):R60.